Effect of graphene oxide dispersion on hydration and carbonation performance of low-clinker cement

Construction and Building Materials 508 (2026) 144950

Contents lists available at ScienceDirect

Construction and Building Materials

journal homepage: www.elsevier.com/locate/conbuildmat

Effect of graphene oxide dispersion on hydration and carbonation performance of low-clinker cement

Suriyaprakash Saravanan [a,b,*], Liming Huang [a,c], Arezou Babaahmadi [a]

[a] Chalmers University of Technology, Department of Civil and Architectural Engineering, Gothenburg 412 96, Sweden
[b] KTH Royal Institute of Technology, Division of Concrete Structures, Stockholm 100 44, Sweden
[c] PNNL, WA 99354, USA

ARTICLE INFO

Keywords:
Graphene Oxide
Polycarboxylate Ether
Low-Clinker Cement
Hydration Kinetics
Early-Age Strength
Carbonation

ABSTRACT

This study demonstrates how polycarboxylate ether-based superplasticizers (PCE) enable graphene oxide (GO) to improve the early hydration and mechanical performance of a low-clinker ternary cement, while also revealing an unexpected trade-off in carbonation behaviour. The ternary system consisted of ordinary Portland cement, slag, and limestone powder. The dispersion state of GO was evaluated through visual observation, ultraviolet-visible spectroscopy (UV-Vis) and dynamic light scattering (DLS), which confirmed that a PCE/GO mass ratio of 10 provided optimal stabilization. Isothermal calorimetry showed that 0.2 wt% GO accelerated hydration most effectively, while mortar testing demonstrated that 0.1 wt% GO increased 1-day compressive strength by 26 %. In-situ X-ray diffraction (XRD) further verified the promotion of early hydration phases. Under accelerated carbonation, however, 0.1 wt% GO increased the initial carbonation rate by 83.7 % without a corresponding increase in the total carbon dioxide (CO_2) uptake, as determined by thermogravimetric analysis (TGA). This paradox suggests that GO may act as a nucleation agent for rapid surface precipitation of calcium carbonate ($CaCO_3$), producing a dense outer layer that restricts further CO_2 ingress. The finding that GO accelerates carbonation kinetics without enhancing total sequestration challenges prevailing assumptions in the literature and provides new guidance for the design of sustainable, nano-engineered, low-clinker binders, requiring a careful balance between early-age performance and long-term durability.

1. Introduction

Cement production contributes approximately 8 % of global anthropogenic CO_2 emissions, making it one of the most significant industrial sources of greenhouse gas emissions [1,2]. This presents a critical challenge for decarbonizing the construction industry and achieving the global climate objectives. Transformative changes in cement production practices are required to meet these goals, particularly through reducing the clinker content in cement, a major source of emissions [3]. One of the most promising strategies to achieve this is the increased utilization of Supplementary Cementitious Materials (SCMs), which replace part of the clinker while maintaining or enhancing the mechanical and durability properties of concrete [4,5].

SCMs such as fly ash, slag, limestone, and silica fume are widely recognized for their ability to improve the sustainability of cement-based materials by reducing clinker usage [6,7]. These materials contribute to long-term strength and durability through pozzolanic reactions, which form secondary calcium silicate hydrate (C-S-H) [4,6]. However, the incorporation of SCMs in higher replacement levels often leads to slower early strength development. This is primarily due to the reduced clinker content and the slower kinetics of pozzolanic reactions [8,9]. The dilution of the cement matrix caused by high SCM replacement further exacerbates this issue, posing challenges in applications where early-age strength is critical, such as precast concrete or high-speed construction projects [10].

Another critical concern in SCM-rich systems is the increase in carbonation rate. Reduced portlandite availability and changes in porosity can make blended cements more susceptible to carbonation compared to traditional Portland cement [11–13]. While carbonation is typically viewed as a durability threat, particularly in reinforced concrete due to the reduction of pH and the risk of steel corrosion [11,14], it is increasingly being recognized as an opportunity for carbon capture in specific contexts [15]. For instance, in unreinforced or surface-exposed concrete elements, accelerated carbonation could contribute to net CO_2

* Corresponding author at: KTH Royal Institute of Technology, Division of Concrete Structures, Stockholm 100 44, Sweden.
E-mail address: sursar@kth.se (S. Saravanan).

https://doi.org/10.1016/j.conbuildmat.2025.144950
Received 28 August 2025; Received in revised form 27 November 2025; Accepted 17 December 2025
Available online 6 January 2026

sequestration, offsetting a portion of the emissions from clinker production [13,15].

Successfully leveraging carbonation for carbon capture requires a controlled approach that maximizes CO_2 uptake while maintaining microstructural integrity and mechanical performance [15]. To address these dual challenges of early strength development and carbonation control, the application of nanotechnology has emerged as a promising solution. Among various nanomaterials, graphene oxide (GO) stands out due to its high surface area, functional groups, and ability to serve as nucleation sites for hydration products [16–18]. However, while its effects on ordinary Portland cement are increasingly understood, its behaviour and impact within complex, SCM-rich ternary systems remain a critical knowledge gap. In ordinary Portland cement systems, GO has been shown to accelerate hydration, leading to increased early strength, densification of the matrix, and improved pore structure [19–21].These enhancements are primarily achieved through two mechanisms: seeding effects, where nanomaterials provide nucleation sites for hydration products, and filling effects, where the materials fill micro-voids in the cement matrix, leading to a denser and more compact structure [22–24]. By modifying the microstructure at the nanoscale, nanomaterials can enhance hydration kinetics and improve the macroscopic properties of concrete [25].

Emerging evidence also suggests that GO may enhance CO_2 sequestration in cementitious systems. While some studies have focused on how GO influences the crystallization and structure of the calcium carbonate that forms during carbonation [26,27], Mishra et al. (2022) demonstrated that GO-modified cement composites exhibited greater CO_2 uptake than control systems, indicating that GO could enable a dual-function binder that both strengthens and sequesters carbon [28]. However, the underlying mechanisms remain unclear, and further validation is needed to determine the extent and reproducibility of this effect across different binder systems.

Despite these promising findings, the effectiveness of GO as a nano-reinforcement is highly dependent on achieving a uniform dispersion of its nanosheets in the cement matrix. GO's stability in aqueous solutions is attributed to its electrostatic repulsion and hydrophilic nature [29,30]. Yet, in the highly alkaline environment of cement pore solutions, the presence of ions such as Na^+ , K^+, OH^-, and Ca^{2+} poses significant challenges for maintaining this stability [31,32]. Calcium ions, in particular, interact with the functional groups of GO, leading to the formation of agglomerates [32,33]. This aggregation, combined with the deoxygenation of GO in alkaline conditions, reduces its effectiveness as a reinforcement and introduces weak zones in the cement matrix [31,34].

To overcome these challenges, researchers have explored various dispersion techniques for GO in cementitious systems. Ultrasonication, which uses high-frequency sound waves to mechanically break up agglomerates, is a commonly used method to achieve stable aqueous suspensions of GO [34,35]. However, ultrasonication alone is often insufficient to maintain stable and uniform dispersion in cement pore solutions due to the complexation of calcium ions with GO [34,35]. Alternative approaches, such as chemical surface modification and the use of dispersing agents, have been proposed. While chemical modification can improve GO stability, it is often complex, time-consuming, and may interfere with cement hydration processes [36–38].

Recent studies suggest that polycarboxylate ether-based superplasticizers (PCE) offer a more practical solution [39,40]. PCE, known for their steric hindrance effects, prevent GO aggregation by adsorbing onto its surface [41]. They are also compatible with cement hydration processes, making them an effective dispersing agent in cementitious environments [38]. Significant progress has been made in understanding the effects of GO on plain cement systems. For instance, studies on OPC and C_3S have consistently shown that well-dispersed GO acts as a nucleation agent, accelerating hydration and leading to a more refined pore structure [38,42,43]. This acceleration has been shown to produce significant gains in early-age compressive and flexural strength. However, the role of GO in more complex blended systems containing SCMs remains largely unexplored.

Specifically, a consensus is emerging in the literature that GO reduces the carbonation rate in ordinary Portland cement systems. This beneficial effect is consistently attributed to the nano-reinforcement capability of GO, which leads to a more refined pore structure, reduced overall porosity, and a denser, less permeable matrix that physically hinders the ingress of CO_2 [44–46]. However, this established behavior in high-clinker OPC systems may not be directly applicable to SCM-rich binders, where the chemical environment and hydration kinetics are fundamentally different [47]. Thus, the interaction between GO and carbonation in low-clinker blended systems remains a critical, unaddressed knowledge gap. Understanding these interactions is essential for developing low-clinker binders that combine the sustainability benefits of SCMs with the performance enhancements provided by GO.

The ternary binder system used in this study was previously characterized by some of the co-authors in terms of its fundamental hydration properties [48,49]. The present work builds upon that foundation but represents a distinct and novel contribution by introducing GO as a nano-additive. The focus of this manuscript is to systematically investigate the dispersion of GO in this specific low-clinker system and to explore its subsequent effects on hydration kinetics, mechanical performance, and, most critically, to report the unexpected paradoxical effect of GO on carbonation, which has not been previously studied.

This study aims to address this gap by investigating the effects of GO on the hydration, early strength development, and carbonation of low-clinker blended cement systems incorporating slag and limestone. Specifically, this study investigates the early-age interactions between GO and cement hydrates in ternary systems using techniques such as visual observation tests, ultraviolet-visible (UV-Vis) spectroscopy, and dynamic light scattering (DLS). Hydration kinetics and total heat evolution during the initial 22 h of hydration are analysed using isothermal calorimetry, while in-situ X-ray diffraction (XRD) monitors real-time hydration compound formation. The compressive strength of GO-modified ternary mortars is evaluated at 1, 3, and 7 days to assess GO's impact on early-age strength development. Finally, the carbon sequestration potential of GO-modified cement paste was analysed by coloration and thermogravimetric analysis (TGA). By linking dispersion quality to hydration, strength, and carbonation performance, this study provides new insight into the design of nano-engineered, low-clinker binders with potential to accelerate the transition toward carbon-neutral construction materials.

2. Materials

2.1. Binder and admixture

In this study, a ternary binder was used, composed of an ordinary Portland cement (CEM I 52.5 R) and two types of SCMs. The cement from Heidelberg Materials, Sweden, and the SCMs included: Slag from Thomas Cement; and limestone powder from Nordkalk (Limus 15). The binder was mixed by the mass proportions of 49 % CEM I, 35 % slag, and 16 % limestone. This composition was selected to represent a typical low-clinker, high-volume SCM cement formulation in line with modern sustainability goals. The chemical composition and Loss on Ignition (LOI) of each component were determined via X-ray fluorescence analysis, with the results presented in Table 1. Detailed characterization including particle size distribution curves of the binder components was provided in previous publications [48,49]. Key fineness parameters are: Blaine fineness values of 525 m^2/kg for the CEM I 52.5 R and 420 m^2/kg for the slag. The limestone powder (Limus 15) has a D50 of 18 μm. PCE supplied by Thomas Concrete Group, Sweden, was employed as a dispersing agent.

Table 1
Chemical composition and LOI of each binder.

Component	CaO	SiO_2	Al_2O_3	Fe_2O_3	MgO	K_2O	Na_2O	Cl	Sulphide	LOI
CEM I 52.5 R (wt%)	62.2	19.6	4.5	3.5	3.5	1.01	0.27	0.07	-	2.5
Slag (wt%)	39.11	36.63	13.56	0.49	8.52	0.57	0.46	0.009	-	1.07
Limestone (wt%)	49.5	9	-	0.3	0.3	0.3	0.1	-	-	40.1

2.2. Graphene oxide

The GO used in this study was supplied by Graphenea SA. as a slurry with a concentration of 20 mg/mL and a bulk density of approximately 1.5 g/cc. The material is a dark brown, odourless liquid with a pH of 1.8–2.2 in a 4 mg/mL dispersion. The elemental composition of GO, as provided by the supplier, is shown in Table 2.

2.3. Simulated pore solution

To evaluate the effect of alkalinity on the stability of GO dispersion, a simulated pore solution was prepared to mimic the chemical environment of cement paste. The solution was created by dissolving $Ca(OH)_2$, NaOH, KOH, and $CaSO_4$ pellets into deionized water. The saturated solution of was filtered by 0.22 μm syringe filter after 24 h and stored in sealed containers to prevent carbonation. The final ionic concentration of the pore solution is shown in Table 3. The measured pH of the solution was determined to be 13, simulating the highly alkaline conditions typical of cement pore solutions.

3. Methods

3.1. Experimental program

The experimental program was designed to systematically evaluate the dispersion of GO and its subsequent effects on the hydration, mechanical properties, and carbonation of the ternary blended cement system. The program involved three main stages: (1) Dispersion Optimisation, where the stability and dispersion of GO in a simulated cementitious environment were evaluated to identify the optimal PCE/GO ratios for stable, high-quality dispersion; (2) Hydration and Mechanical Properties Analysis, which used these optimal ratios to investigate the impact of GO on hydration kinetics and early-age strength, with the goal of identifying the most effective GO-PCE system; and (3) Carbonation Analysis, where these optimized samples were then assessed for their carbon sequestration performance. The overall workflow of this three-stage program is illustrated in the flowchart in Fig. 1.

3.2. Preparation of GO suspensions

GO suspensions were prepared by diluting a GO slurry (20 mg/mL) to target concentrations. The diluted suspensions were subjected to 30 min of sonication in a Bandelin Sonorex TK52 ultrasonic processor (60 kHz, Bandelin Electronic, Germany). PCE was added to the suspensions at mass ratios of 0, 5, 10, 15, and 20, which were designated as PCE0, PCE1, PCE2, PCE3, and PCE4, respectively. This range of PCE/GO ratios and GO concentrations was chosen based on literature recommendations to investigate the spectrum from insufficient to potentially excessive dispersant and nano-additive levels. The suspensions were sonicated for an additional 30 min to ensure uniform dispersion. The water in the sonication bath was replaced every 15 min to maintain a temperature of approximately 25°C.

Table 2
Elemental composition of the GO as provided by the manufacturer.

Element	Carbon	Oxygen	Hydrogen	Nitrogen	Sulphur
%	49–56	41–50	1–2	0–1	0–1

Table 3
Ionic concentrations of the simulated pore solution.

$Ca(OH)_2$ (g/l)	NaOH (g/l)	KOH (g/l)	$CaSO_4$ (g/l)	Ca^{2+} (mol/l)	Na^+ (mol/l)	K^+ (mol/l)	$(SO_4)^2$ (mol/l)
Sat.	3.560	10.475	9.938	0.006	0.089	0.159	0.073

3.3. Physical observations of dispersion stability

The stability of the prepared GO suspensions was evaluated in the simulated pore solution. The suspensions were diluted to a final GO concentration of 1 mg/mL and transferred to sealed glass vials. The samples were then visually inspected for sedimentation and agglomeration immediately after mixing and at intervals of 1, 12, and 24 h.

3.4. Ultraviolet–visible spectroscopy (UV-Vis)

UV-Vis spectroscopy was conducted to qualitatively assess the dispersion of GO. Measurements were conducted over a wavelength range of 190–500 nm within 10 min of sample preparation. he GO suspensions were diluted to 0.02 mg/mL before analysis to ensure absorbance values were within the optimal range. A baseline correction was performed using a pure PCE solution to isolate the absorbance spectrum of GO.

3.5. Dynamic Light Scattering (DLS)

DLS analysis was performed using a Litesizer™ 500 (Anton Paar) to determine the particle size distribution of GO in both aqueous and simulated pore solutions. Measurements were first conducted on GO suspensions at a concentration of 1 mg/mL in water, followed by a diluted concentration of 0.5 mg/mL in simulated pore solutions.

3.6. Measurement of hydration kinetics

The early-age hydration heat was measured using a Calmetrix I-Cal Ultra. Samples were prepared by mixing 3 g of binder with 1.5 g of predispersed GO solution using a vortex mixer (Whirli VIB 2, InterMed). The experiments were carried out at a controlled temperature of 20 °C. The prepared samples were loaded into ampoules, and data collection began after the first hour to exclude heat signals influenced by external mixing. Hydration data were recorded at 5-second intervals. To ensure consistent comparison with the phase evolution analysis, the hydration data was evaluated over the first 22 h.

3.7. Mechanical strength evaluation

Compressive strength tests were conducted on mortar specimens with a binder-to-sand ratio of 1:3. Fresh mortar was cast into 40 mm cubic molds, covered by plastic film, and demoulded after 24 h. The specimens were cured in a water bath at 20 ± 2 °C until the testing days of 1, 3, and 7 days. A MATEST Universal Testing Machine (300 kN capacity) was used to apply a compressive load at a rate of 1.250 kN/s. Three replicate samples were tested for each mixture.

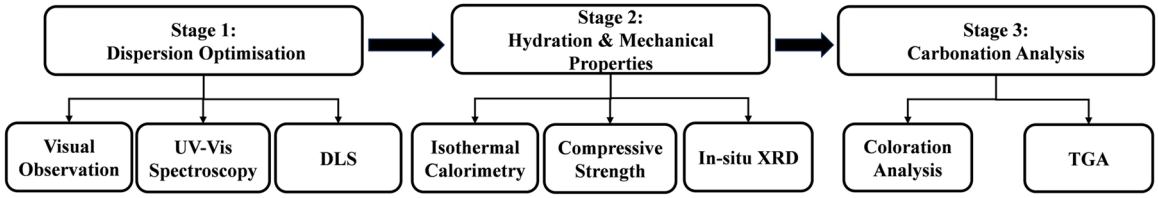

Fig. 1. Flowchart of the experimental program, outlining the three main stages of the study.

3.8. X-ray diffraction (XRD)

The real-time evolution of crystalline hydration phases was monitored using in-situ XRD. Freshly mixed pastes were placed in a sample holder, and the surface was covered with a 7.5 μm Kapton polyimide film to prevent drying. Measurements were conducted using a Bruker D8 Discover diffractometer with CuKα radiation (40 kV, 40 mA). Diffraction patterns were recorded continuously for 22 h over a 2θ range of 7°–50° with a step width of 0.020° and a counting time of 0.5 s per step. A total of 2151 patterns were recorded over 22 h, with each pattern requiring approximately 90 s. The diffraction patterns were analysed using the DIFFRAC.EVA software.

3.9. Carbonation testing and evaluation

Paste samples were exposed to accelerated carbonation in a chamber controlled at 2.9 vol% CO_2, 22 ± 2°C, and 53 ± 5 % relative humidity. For each mixture, four replicate paste samples were prepared and tested. The carbonation depth was measured every 7 days for 28 days by splitting the samples and spraying the freshly exposed surface with a 1 % thymolphthalein pH indicator solution. After 42 days, when coloration indicated complete carbonation, TGA was performed on the samples using a Mettler Toledo TGA/DSC 1 by heating approximately 20–30 mg of powdered sample from 25 to 1000°C at a rate of 10 °C/min under a nitrogen atmosphere. The contents of calcium hydroxide (CH), calcium carbonate ($CaCO_3$), and the total CO_2 uptake were calculated from the TGA data using the following Eqs. (1)-(3) [28,50]:

$$CH(g/100g) = \frac{M_{400} - M_{500}}{M_{105}} \times 4.1 \times 100 \quad (1)$$

$$CaCO_3(g/100g) = \frac{M_{525} - M_{900}}{M_{105}} \times 2.27 \times 100 \quad (2)$$

$$CO_2 uptake(\%) = \frac{M_{CO_2-carbonated}\ (wt\%)}{100 - M_{CO_2-carbonated}\ (wt\%)} \times 100 \quad (3)$$

In these equations, $M_{105}, M_{400}, M_{500}, M_{525}$, and M_{900} represent the mass of the sample at the corresponding temperatures. The value 4.1 is the molar mass ratio of $Ca(OH)_2$ to H_2O, and 2.27 is the molar mass ratio of $CaCO_3$ to CO_2. The term $M_{CO_2-carbonated}$ refers to the mass loss percentage from the decomposition of $CaCO_3$ relative to the dry mass of the sample at 105 °C.

4. Results and discussion

4.1. Characterization of GO dispersion in simulated pore solution

4.1.1. Stability and dispersion of GO in a simulated cement environment

The stability of GO dispersion in the chemical environment of early-age cement hydration was evaluated by introducing a pure GO aqueous suspension into a simulated cementitious pore solution. As shown in Fig. 2, GO remains well-dispersed in water (a) but undergoes visible agglomeration in the pore solution (b). This visible agglomeration is consistent with the well-established mechanism of Ca^{2+} cross-linking and ionic destabilization in alkaline pore solutions, as discussed in the introduction [30–33,51]. Consequently, achieving a stable GO suspension in water does not ensure the same dispersion state in the highly alkaline cementitious environment. The formation of GO agglomerates in cement pore solutions can significantly diminish its effectiveness as a nano-reinforcement, highlighting the need for appropriate dispersion strategies to maintain GO stability throughout the hydration process [31,32].

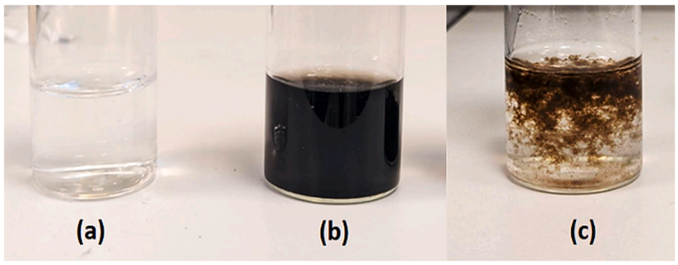

Fig. 2. (a) Simulated pore solution, (b) GO (1 mg/mL) in deionized water, and (c) GO in pore solution showing agglomeration.

Fig. 3 presents a visual assessment of the stability of GO dispersion over time, when stabilized with various mass ratios of PCE to GO. At the initial observation (0 h), all samples exhibited no signs of agglomeration, underscoring the crucial role of PCE in stabilizing the GO suspension. The introduction of PCE to the cementitious matrix facilitates the attachment of carboxylic acid groups onto the GO surface, thereby increasing the presence of hydrophilic groups [41]. This modification mitigates the van der Waals forces between GO sheets, subsequently elevating the energy required to separate them from the cement matrix [39,41]. The incorporation of PCE into the cementitious system yields two notable benefits: it enhances the fluidity of the mixture without adversely affecting the final strength of the cement, and it ensures the uniform dispersion of GO throughout the matrix [38,39].

At a PCE/GO mass ratio of 5, the GO suspension initially remained stable for up to one hour before agglomeration began, eventually leading to complete settling within 12 h. By this point, the supernatant was visibly clear, indicating that the PCE dosage was insufficient to effectively coat the GO flakes to prevent aggregation [39,52]. Similarly, GO suspensions with PCE/GO ratios of 10 and 20 exhibited limited dispersion stability. Although these suspensions maintained a relatively stable dispersion for the first hour, partial agglomeration soon followed, resulting in a thin layer of settled GO at the bottom.

While a PCE/GO ratio of 10 provided certain dispersion stability, it was ultimately inadequate to maintain after 1 h. Over time, chemical interactions between GO and the pore solution overpowered the steric hindrance imparted by PCE, leading to progressive agglomeration [41,52]. Increasing the ratio to 20 introduced excess PCE molecules, which likely triggered steric repulsion among PCE molecules themselves. This repulsion effect may have caused PCE desorption from the GO surface, reducing its effectiveness as a dispersing agent [40,53]. In contrast, a PCE/GO mass ratio of 15 demonstrated excellent macroscopic dispersion stability, with no visible sedimentation in the simulated pore solution over a 24-hour period. While there was an observed increase in optical density of the suspension over time, indicative of some degree of GO agglomeration, the steric repulsion provided by this optimal PCE mass ratio effectively prevented sedimentation. To quantitatively

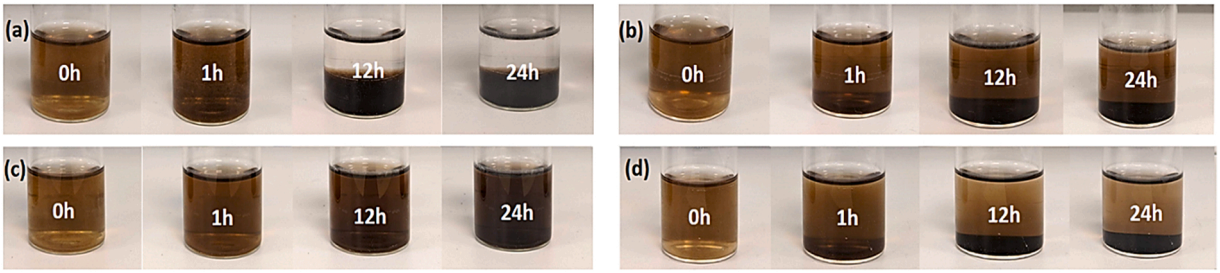

Fig. 3. Visual stability of GO suspensions in simulated pore solution over 24 h with varying PCE/GO mass ratios: (a) 5, (b) 10, (c) 15, and (d) 20.

confirm these visual observations, UV-Vis spectroscopy and DLS were employed.

4.1.2. Spectroscopic analysis of GO dispersion

In the case of single-layered GO, the UV-Vis spectrum typically exhibits a distinct peak at 230 nm and a shoulder at approximately 310 nm [54]. The absence of these characteristic peaks for PCE0, as shown in Fig. 4, indicates the missing of GO single layer under the highly alkaline conditions (~pH 13) of the cementitious environment, which facilitates the reduction of GO through the ionization and consumption of oxygen-containing functional groups on its surface [55,56]. This reduction process disrupts the $\pi-\pi^*$ and $n-\pi^*$ plasmon transitions, which are associated with aromatic $C-C$ bonds and oxygen functionalities, respectively. These transitions are responsible for the UV-Vis spectral features observed at 230 nm and 310 nm [55,57]. However, thick-layered or aggregated GO lacks these features, as the nanosheets no longer efficiently absorb light due to reduced surface exposure [58].

As shown in Fig. 4, the absorbance at 310 nm (the characteristic shoulder peak) for PCE1, PCE2, PCE3, and PCE4 was 0.34, 0.56, 0.44, and 0.36, respectively. These values are significantly higher than that of PCE0, according to Beer-Lambert's law, higher absorbance values correspond to better dispersion, as well-dispersed nanosheets efficiently absorb light in the UV-Vis region [23,59], reflecting improved dispersion of GO due to the presence of PCE. At a PCE/GO mass ratio of 5, the absence of a distinctive shoulder peak and the lowest absorbance value suggest that the PCE concentration was insufficient to adequately coat the basal planes of GO. This insufficient coverage results in inadequate repulsive forces between GO flakes, allowing Van der Waals attractions to dominate and cause aggregation [39].

When the PCE/GO mass ratio was increased to 10, a 62.17 % increase in the shoulder peak intensity indicates an enhancement of GO dispersion. However, the further increase of the PCE/GO ratio to 15 led to a 20.32 % reduction in the absorption intensity at 310 nm, with an additional 19.34 % decline observed at the PCE/GO ratio of 20. This decrease can be attributed to the formation of micelles at high PCE concentrations. The micelles increase the osmotic pressure of the suspension, preventing effective separation of GO flakes and promoting their re-aggregation [60,61]. Despite a large increase in PCE concentration from PCE1 to PCE4, the shoulder peak intensity differed by only 4.06 %, suggesting a saturation effect in PCE's ability to stabilize GO [60,62].

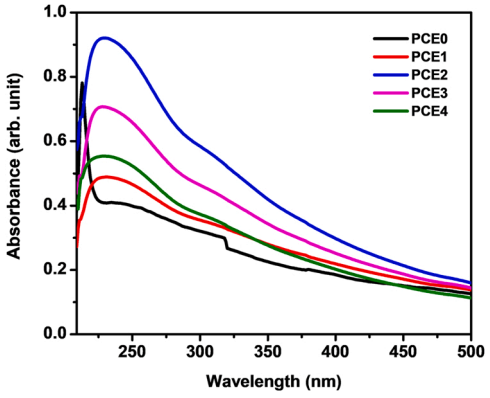

Fig. 4. UV-Vis absorption spectra for GO suspensions in simulated pore solution with different PCE/GO mass ratios.

Interestingly, the peak at 230 nm demonstrated the highest absorption intensity for PCE/GO ratio of 10, supporting that moderate PCE concentrations are optimal for dispersing GO nanosheets in the pore solution. Lai et al. [58] suggest that UV-Vis spectroscopy can also differentiate the dispersion states based on the number of GO layers. Single-layered GO exhibits sharp peaks at 230 nm, while thicker layers or aggregated GO show diminished features. The observed trend in Fig. 4, which indicates the degree of GO dispersion follows the order PCE2 > PCE3 > PCE4 > PCE1 > PCE0, was then verified by particle size analysis.

4.1.3. Particle size analysis of GO dispersion

The particle size measurements of GO dispersion conducted using DLS assumed that the particles were spherical, limiting the instrument's ability to provide the absolute size of GO flakes. However, despite this limitation, the measurements offered a rapid and efficient comparative assessment of size distribution [63,64]. Fig. 5(a) and (b) show the particle size distributions of GO suspensions with various PCE dosages in water and a simulated pore solution, respectively. The influence of ultrasonication on GO dispersion was evaluated by comparing the particle size distributions of GO suspension in water. In Fig. 5a, the Raw GO sample represents the as-received GO suspension without sonication, showing a broad particle size range from 1976 nm to 4818 nm. In contrast, the PCE0 sample represents the same GO suspension after 60 min of sonication (without PCE added). Following the total 60-minute sonication period, the size distribution shifted significantly, with a reduction in range to 612-3973 nm, confirming the effectiveness of our chosen duration in exfoliating aggregated GO flakes. And the appearance of a new peak at 168 nm to 426 nm, indicates the presence of few-layered GO, confirming the effectiveness of sonication in exfoliating aggregated GO flakes. This result aligns with findings by Lai et al., who reported that ultrasonication improves the dispersion of GO by breaking down agglomerated clusters into smaller, well-dispersed flakes [58].

In water (Fig. 5a)., the size distribution curves for all GO suspensions exhibit broad peaks, indicating a wide range of particle sizes with low relative frequency intensity. However, in the pore solution (Fig. 5b), PCE0 (GO without PCE) displayed no distinct peaks due to severe agglomeration.

In suspensions containing PCE (PCE1-PCE4), the particle size distributions displayed well-defined peaks in both water and pore solution, reflecting the steric hindrance provided by PCE, which prevented GO sheets from aggregating [41,65]. However, the degree of dispersion was influenced by the PCE concentration. For PCE1, the particle size ranged from 1216 nm to 4443 nm in water, with edge thickness measurements between 56 nm and 77 nm. In the pore solution, the particle size distribution narrowed to 1034 nm–1550 nm, and the disappearance of the lateral peak was likely caused by cross-linking effects. These

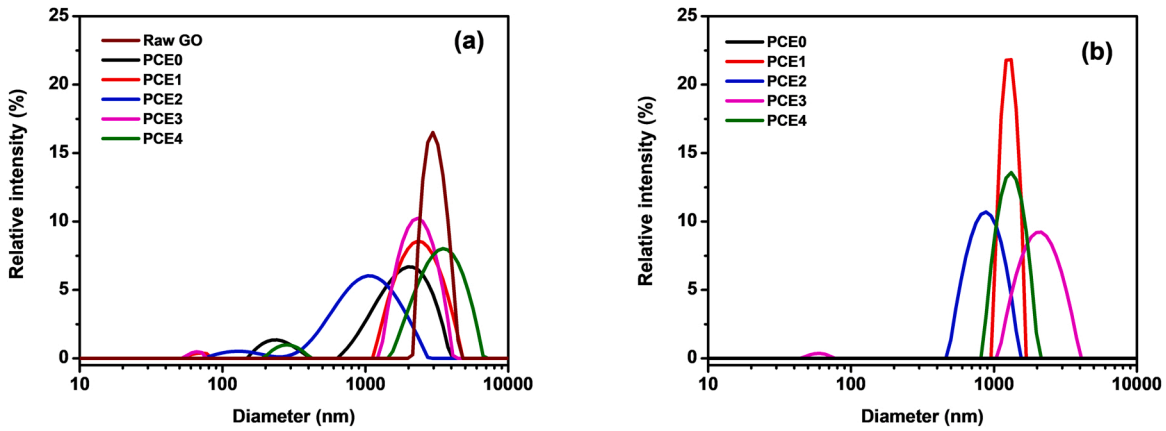

Fig. 5. Particle size distribution of GO suspensions in (a) deionized water and (b) simulated pore solution. Note: In (a), "Raw GO" is the non-sonicated sample, while "PCE0" is the sonicated sample without PCE.

cross-linking interactions can occur through bridging between GO sheet edges, intercalation between basal planes, or hydrogen bonding between oxygen functional groups and interlamellar water molecules [66,67]. Despite the steric hindrance provided by PCE, the concentration in PCE1 appeared insufficient to fully coat and protect the GO sheets, resulting in a moderate aggregation [39,68].

Among all tested concentrations, PCE2 demonstrated the best dispersion. In water, the particle size range for PCE2 was 77 nm to 2733 nm, with the smallest hydrodynamic diameter of 908.09 nm, while in the pore solution, the size distribution shifted to 498 nm to 1429 nm. This reduction in particle size highlights the optimal balance between steric hindrance and particle stabilization provided by PCE2. The superior performance of PCE2 in minimizing aggregation aligns with the trends observed in the UV-Vis spectra, which also indicated the most effective stabilization at this dosage.

At higher PCE concentrations (PCE3 and PCE4), the particle sizes increased, indicating a decline in dispersion efficiency. For PCE3, the particle size range was 1318 nm to 4098 nm in water and 1121 nm to 3779 nm in the pore solution, while for PCE4, the size ranged from 1550 nm to 6662 nm in water and 879 nm to 1976 nm in the pore solution. This trend can be attributed to the formation of micelles at high PCE concentrations, which increases the osmotic pressure of the suspension and prevents effective interaction between PCE molecules and GO sheets [60,69]. As a result, re-aggregation of GO flakes occurs, diminishing the stabilization effect of PCE.

In summary, the combined results from visual observation, UV-Vis spectroscopy, and DLS analysis are integrated in Table 4. These results indicate that while a PCE/GO ratio of 10 provided the optimal initial dispersion, a ratio of 15 offered the best long-term stability against sedimentation. This understanding informed the selection of PCE dosages for the subsequent hydration and performance evaluations.

4.2. Impact of GO and PCE on early hydration kinetics

4.2.1. Effect of GO concentration on hydration

Fig. 6 presents the heat evolution curves for ternary binder pastes with varying GO concentrations, without PCE (a, b) and with a fixed PCE/GO mass ratio of 15 (c, d). This ratio of 15 was selected for this initial test series, as it demonstrated the best long-term dispersion stability in our 24-hour visual assessment (Section 4.1.1), which was considered critical for the extended hydration measurement. In the legends, samples are labelled by their GO dosage (e.g., 0.05 % GO). The first experimental series, conducted without any dispersing agent (Fig. 6a, b), confirms that GO enhances the hydration reaction, as all GO-incorporated samples show a higher hydration heat rate and cumulative heat release than the control. The heat evolution rate curves (Fig. 6a) are characterized by two distinct peaks at about 4 and 8 h, respectively. With increase in GO content, the second shoulder peak, associated with C_3A hydration, shows a more significant increase in magnitude than the first peak (C_3S reaction), suggesting the nucleation effect of GO is more pronounced for C_3A hydration in this blended system [18,24]. A plausible mechanism for this is the interaction between GO's abundant oxygen-containing functional groups and the dissolved aluminate and sulphate ions in the pore solution. These functional groups may act as preferential nucleation sites for aluminate hydrate phases (e.g., ettringite), thereby accelerating gypsum consumption and the overall C_3A reaction pathway more significantly than the C_3S reaction [18,24]. The cumulative heat curves (Fig. 6b) show that while all GO-pastes exhibited lower cumulative heat than the control during the first 8 h due to a dilution effect, they surpassed the control at later stages. The increases in cumulative hydration heat relative to the reference sample were as follows: 0.09 J/g for 0.05 % GO, 1.82 J/g for 0.1 % GO, 4.28 J/g for 0.2 % GO, and 4.26 J/g for 0.4 % GO. The sample with 0.2 wt% GO exhibited the most favourable reaction, confirming its strong nucleation effect.

Table 4
Summary of GO dispersion characterization results.

Sample	PCE/GO Ratio	Visual Stability (24 h)	UV-Vis Result	DLS Particle Size (in pore solution)	Key Finding
PCE0	0	Severe agglomeration & sedimentation	Lowest absorbance; aggregated	No distinct peaks (severe agglomeration)	Unstable without PCE.
PCE1	5	Complete settling within 12 h	Low absorbance; poor dispersion	1034–1550 nm (moderate aggregation)	Insufficient PCE.
PCE2	10	Partial agglomeration; some settling	Highest absorbance; best initial dispersion	Smallest size (498–1429 nm)	Optimal initial dispersion.
PCE3	15	No visible sedimentation	High absorbance; good dispersion	Increased size (1121–3779 nm)	Best long-term stability.
PCE4	20	Partial agglomeration; some settling	Decreased absorbance (re-aggregation)	Increased size (879–1976 nm)	Excess PCE causes re-aggregation.

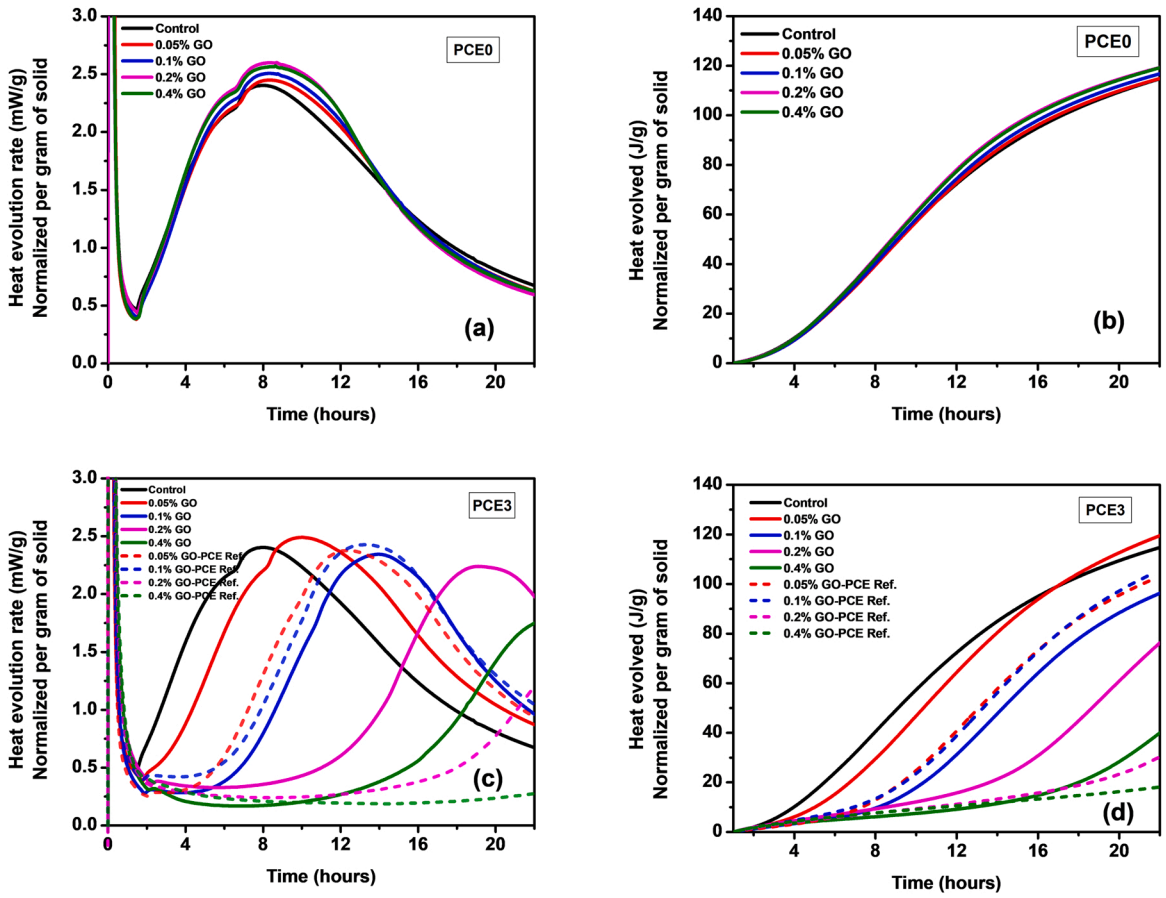

Fig. 6. Effect of GO concentration on the heat of hydration: (a, b) without PCE, and (c, d) with a constant PCE/GO mass ratio of 15.

In the second series, a constant PCE/GO mass ratio of 15 was maintained (Fig. 6c, d). As the GO dosage increased, the corresponding PCE concentration also increased, leading to a drastic increase in the induction period. This behaviour is commonly observed in PCE-containing systems, as higher dosages of PCE act as retarders during cement hydration [70]. However, when compared to the corresponding PCE-only reference samples (shown as dotted lines and labelled as 0.05 % GO-PCE Ref, etc., in the legend), the net effect of GO modification was clearly acceleratory. All GO-modified pastes exhibited a significantly shorter induction period and an earlier onset of the acceleration phase than their PCE-only counterparts, confirming GO's ability to counteract the retarding effects of PCE by promoting early-stage nucleation. This comparison clarifies that in this ternary system, GO does not amplify but rather moderates the retarding behavior of the PCE. Among all GO dosages, the sample with 0.2 wt% GO demonstrated the highest increase in total heat release, with a 1.45-fold rise compared to its PCE reference sample. Based on these combined findings, 0.2 wt% GO was identified as the optimal dosage.

4.2.2. *Effect of PCE concentration on hydration*

Fig. 7 shows the influence of PCE concentration on the hydration of pastes containing a fixed GO content. The first series of experiments with a low GO content of 0.05 wt% (Fig. 7a and b), was selected based on previous studies that identified this concentration as effective for C-S-H formation [71–73]. In the PCE0 sample (no PCE), the heat evolution rate increased in first and second can be attributed to GO's high surface reactivity, which facilitates water molecule attraction, nucleation site formation, and early precipitation of C-S-H and CH hydration products, thereby accelerating hydration [18,28]. However, However, the rate of heat evolution began to decrease after 15 h, indicating a slowing of the later-age hydration as the reaction entered the deceleration phase. The addition of PCE fundamentally altered this behaviour. As shown in Fig. 7a, increasing the PCE dosage extended the induction period, reduced the heat flow rate during the acceleration phase, and delayed the time to maximum heat flow. Despite this initial retarding effect, the cumulative heat curves in Fig. 7b show that the total heat release was higher for samples with PCE/GO ratios of 5, 10, and 15 (PCE1, PCE2, and PCE3) compared to the control. This indicates that while PCE initially delays hydration, the improved GO dispersion it provides leads to a more efficient overall reaction at later stages. In contrast, the PCE4 sample showed a significantly prolonged induction period and much lower total heat evolution, suggesting that excessive PCE acts as a retarder, slowing down hydration. Among all samples in this series, the one with a PCE/GO ratio of 15 (PCE3) exhibited the highest total heat evolution, making it the optimal dosage for balancing dispersion and hydration enhancement.

A similar trend was observed in the second series for pastes containing the optimal 0.2 wt% GO (Fig. 7c, d). A notable increase in the induction period was observed with increasing PCE dosage. This delay is primarily due to the rise in activation energy required for the nucleation and growth of hydrates in the presence of PCE [74]. Three key mechanisms have been proposed to explain how PCE molecules inhibit hydration: (1) formation of complexes with Ca^{2+} ions in the pore solution, (2) adsorption onto the surface of anhydrous cement grains, hindering hydration product nucleation, (3) restriction of ion movement at the cement-solution interface [70]. Despite this extended induction period, the total heat evolution curve indicates that the sample with a PCE/GO ratio of 15 (PCE3) produced the highest increase in total heat, achieving a 1.37-fold rise compared to its corresponding PCE-only reference sample (shown as dotted lines and labelled as PCE3 Ref in the legend). This significant increase suggests a high potential for strength development, as greater total heat release typically correlates with improved

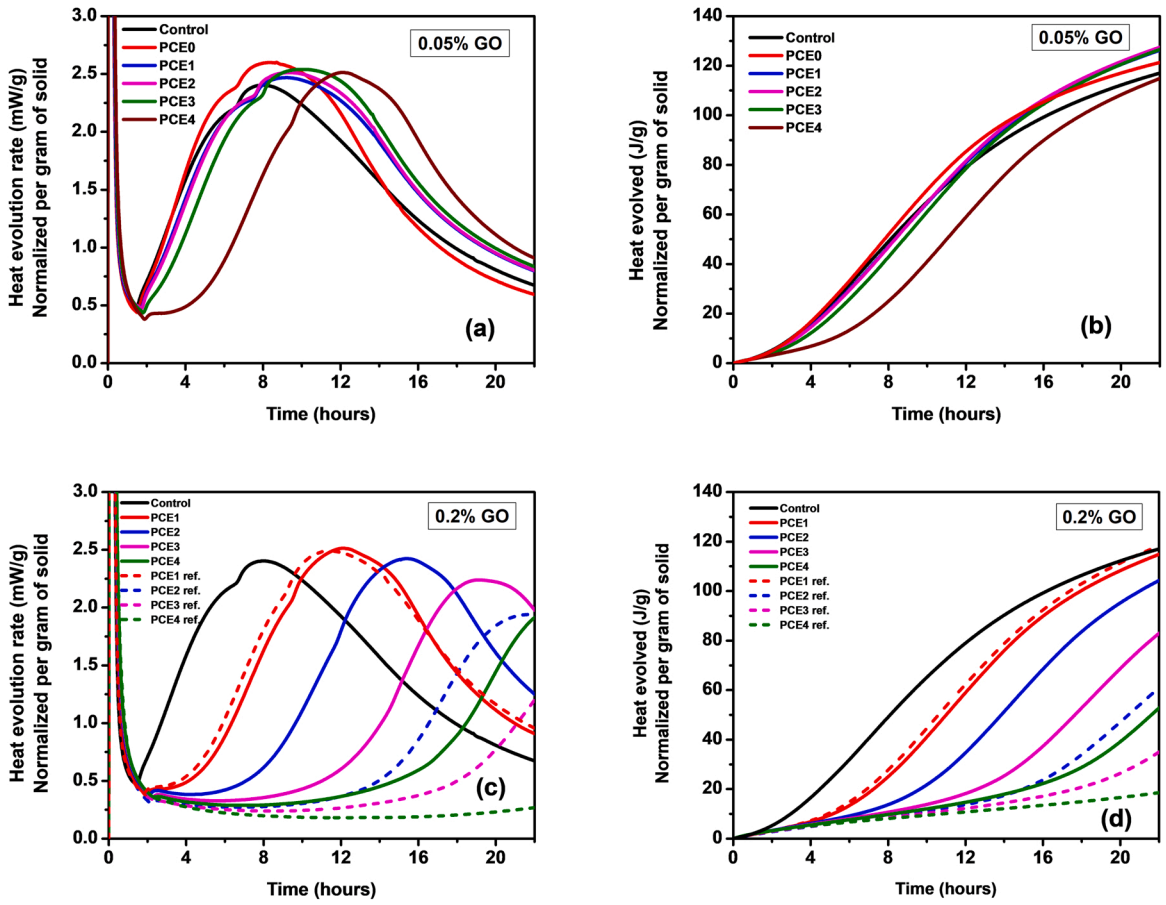

Fig. 7. Effect of PCE concentration on the heat of hydration for pastes containing (a, b) 0.05 wt% GO and (c, d) 0.2 wt% GO.

microstructure formation and early-age strength gain. Although the total heat release remained lower than the additive-free control, these combined results indicate that a PCE/GO ratio of 15 (PCE3) provides the optimal balance for enhancing hydration in GO-modified systems.

4.2.3. Optimisation of the GO-PCE system

The final optimisation experiments, designed to identify the ideal system for mechanical testing, are presented in Fig. 8. To counteract the prolonged induction period observed with high PCE dosages in the previous sections, the PCE concentration was adjusted in proportion to the GO dosage. Given that the GO concentration was increased fourfold (from a 0.05 % to a 0.2 wt% base), the original PCE/GO mass ratios (5, 10, 15, and 20) were correspondingly divided by four. Thus, the new ratios tested in Fig. 8a and b are 1.25, 2.5, 3.75, and 5.

As shown in Fig. 8a, incorporating these adjusted PCE concentrations noticeably shortened the induction period for all GO-containing samples. Among them, the sample with a PCE/GO ratio of 1.25 (PCE1/4) exhibited the highest peak heat rate intensity, indicating an optimal nucleation effect at this combination. In contrast, the other blends demonstrated a lower initial nucleation impact, leading to a retarded heat flow rate during the first 10 h. However, at later ages, these mixtures exhibited higher heat flow rates than the control.

The cumulative heat curve (Fig. 8b) shows that the total heat evolved in the PCE1/4 sample was higher than both the GO-only sample (PCE0) and the control, with an 8 % increase in cumulative heat at 22 h, which can be attributed to the higher number of dispersed cement particles available for hydration [75]. The well-dispersed GO played a catalytic role in cement hydration, primarily due to two factors: (1) the oxygen-containing functional groups on GO, which provide adsorption sites for water and cement particles, facilitating nucleation, and (2) GO-associated water molecules, which act as a reservoir and transport channel, improving hydration efficiency [19,76]. With the optimum PCE concentration established, the next phase of experimentation focused on identifying the best GO concentration for mechanical property analysis.

Following this, the second optimisation series was conducted to identify the best GO concentration for mechanical property analysis, with the results presented in Fig. 8c and d. In this series, pastes evaluated with varying GO concentrations at a constant PCE/GO mass ratio of 1.25. The sample labelled 0.2 % GO (No PCE) is included for comparison to show the effect of adding PCE. The rate of heat flow curves are shown in Fig. 8c. The control mixture exhibited a main peak heat flow intensity of 2.22 mW/g. The peak intensity increased for GO dosages of 0.05 %, 0.1 %, and 0.2 %, but decreased for 0.8 %. The observed increase in peak heat flow with low-to-moderate GO concentrations is attributed to GO's nucleation effect, which facilitates the growth of hydration products, particularly C-S-H, by providing preferential nucleation sites due to its high surface energy and hydrophilic functional groups [77–79]. Interestingly, Li et al. [18] reported that incorporating 0.02 wt% GO in cement paste significantly impacted hydration peak timing, using 0.025 wt% GO in this study did not show the same effect. This discrepancy could be attributed to the retarding effect of the relatively high PCE dosage used in this series, which likely offset the accelerating effect of GO at very low concentrations.

At higher GO dosages of 0.4 % and 0.8 %, the fixed PCE concentration was insufficient to prevent GO agglomeration, which is reflected in the diminished performance shown in the cumulative heat curve in Fig. 8d. This occurs because the low PCE concentration cannot sufficiently coat the basal planes of the higher amount of GO, leading to inadequate repulsive forces to counteract the Van der Waals attractions

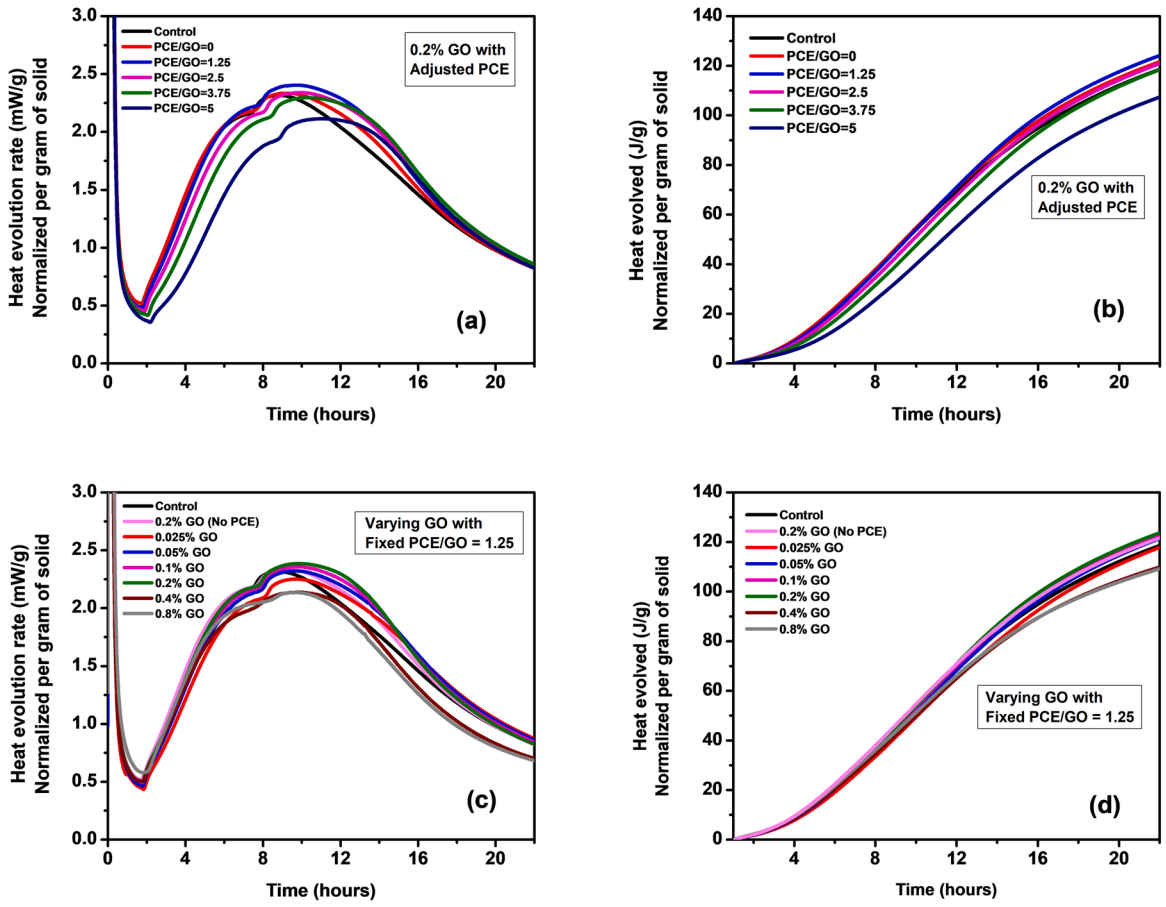

Fig. 8. Optimisation of the GO-PCE system: (a, b) heat of hydration for 0.2 wt% GO with adjusted PCE/GO ratios, and (c, d) for varying GO concentrations with a fixed PCE/GO mass ratio of 1.25.

between the GO flakes [39]. This confirms that early hydration enhancement depends critically on achieving the correct balance between the GO dosage and the PCE concentration.

4.2.4. *Analysis of hydration peak intensity and time*

To provide a consolidated view of the hydration kinetics, the peak intensity and the time to reach the main hydration peak were extracted from the heat evolution curves and are presented in Fig. 9.

Fig. 9a shows the effect of the PCE/GO ratio on the hydration peak for pastes with fixed GO contents of 0.05 wt% and 0.2 wt%. A clear trend is observed for the peak time (blue axis): as the PCE/GO ratio increases, the time to reach the peak is significantly delayed for both series. For the 0.2 % GO series (triangles), the peak time increases from approximately 9 h with no PCE to over 22 h at a PCE/GO ratio of 20. This directly confirms the strong retarding effect of PCE on the hydration reaction. The peak intensity (red axis) shows a more complex trend. For the 0.2 % GO series, the intensity is maximized at a low PCE/GO ratio of 1.25, suggesting that this concentration provides the optimal dispersion to accelerate the reaction rate without a significant retarding effect. At higher PCE/GO ratios, the retarding effect begins to dominate, leading to a reduction in the peak reaction rate.

Fig. 9b illustrates the effect of GO dosage on the hydration peak for

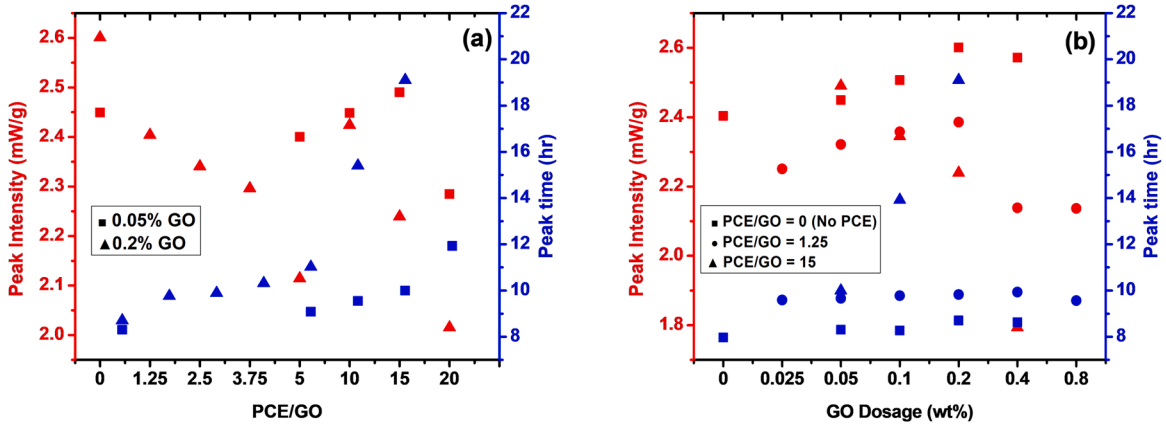

Fig. 9. Analysis of hydration peak intensity and time as a function of (a) PCE/GO ratio and (b) GO dosage.

three different dispersant systems: no PCE (PCE0), an optimized low PCE content (PCE/GO = 1.25), and a high PCE content (PCE/GO = 15). For all three series, the peak intensity (red axis) generally increases as the GO dosage rises from 0 to 0.2 wt%, after which it declines at higher dosages (0.4 % and 0.8 %). This trend consistently demonstrates that 0.2 wt% GO is the optimal concentration for maximizing the rate of hydration, regardless of the PCE content. The data also reinforces the dual role of GO; its nucleation effect enhances the reaction rate up to an optimal point, beyond which agglomeration and insufficient dispersion lead to diminished performance

This analysis confirms that the acceleration of hydration is dependent on a synergistic balance between the GO dosage and PCE concentration, with an optimal system achieved at 0.2 wt% GO and a low PCE/GO ratio.

4.3. Impact on mechanical properties and phase evolution

4.3.1. Early-age compressive strength

The results presented in Fig. 10 indicate that at 1 day, the inclusion of 0.1 wt% GO in the cement paste significantly enhanced compressive strength by 26 % compared to the reference sample. However, increasing the GO concentration to 0.4 wt% resulted in a 26.7 % reduction, suggesting that excessive GO negatively impacts early-age mechanical performance. Meanwhile, at 0.2 wt% GO, the compressive strength exhibited negligible variation, indicating that this concentration had minimal influence on the mechanical properties of the cementitious material. These results clearly demonstrate the high sensitivity of early-age strength to the GO dosage, with an optimal 'window' of performance.

This finding that 0.1 wt% GO yields the optimal mechanical performance appears to contradict the calorimetry data (discussed in Section 4.2) which identified 0.2 wt% GO as the optimal dosage for hydration kinetics. This is not an inconsistency, but rather a key finding: the optimal dosage for accelerating the chemical reaction is not necessarily the same as the optimal dosage for the final mechanical strength. This suggests that while 0.2 wt% GO accelerates hydration, it may also introduce minor agglomeration or microstructural inefficiencies that are detrimental to strength. In contrast, 0.1 wt% GO provides the best balance between hydration enhancement and a well-dispersed, integral microstructure.

At 3 days, a continued increase in compressive strength was observed, with 24.6 % and 18.8 % enhancements for cement pastes containing 0.1 wt% and 0.2 wt% GO, respectively. However, the 0.4 wt % GO mixture showed a 24.9 % decrease relative to the control, further emphasizing that higher GO dosages can have an adverse effect on strength development. Across all GO-modified samples, the maximum compressive strength at 7 days was achieved with 0.1 wt% GO,

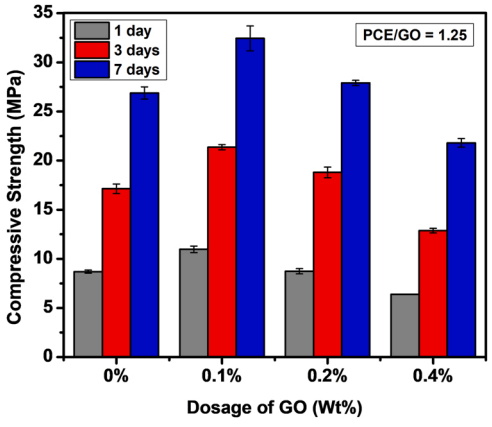

Fig. 10. Compressive strength development of GO-modified mortar at 1, 3, and 7 days.

highlighting its effectiveness in improving early-age performance. The enhancement in compressive strength at lower GO dosages can be attributed to the nucleation effect of well-dispersed oxygen-functionalized graphene oxide, which accelerates hydration by providing additional nucleation sites for hydration products [17,25]. It reduces porosity by filling voids within the cement matrix, leading to a denser microstructure and improved mechanical performance. Under mechanical loading, the GO-reinforced binder matrix transfers stress from the cement matrix to the GO sheets through interfacial interactions. Since graphene-based materials possess significantly higher tensile strength than cement, this load-transfer mechanism improves the structural integrity of the composite [80].

As hydration progresses, the compressive strength of all samples increases due to the continued formation of hydration products within the initial water-occupied spaces. However, in GO-blended mixes with higher GO dosages (0.4 wt%), a decline in compressive strength suggests that poor dispersion of GO may hinder early-stage hydration. This reduced strength is likely due to GO agglomeration, which disrupts the packing efficiency of hydration products and inhibits optimal space-filling within the matrix [32]. Furthermore, at higher GO dosages, insufficient PCE concentrations may limit steric stabilization, increasing the likelihood of GO flake overlap rather than random dispersion. Similar findings by Saafi et al. [81] confirmed that excessive GO sheets tend to cluster rather than remain well-dispersed, compromising their reinforcing ability. This clearly suggests that the optimal dosage window for GO is narrow and critically dependent on achieving adequate dispersion, highlighting the need for further research into optimizing GO-dispersant co-additives for practical use.

Beyond dispersion effects, GO may also influence the composition and morphology of cement hydration products, thereby affecting mechanical properties. Research has shown that various forms of C-S-H exhibit distinct chemical structures and morphologies, which contribute differently to cement strength [82]. Given the observed variations in compressive strength, it is essential to investigate the interactions between GO and hydration products over time. To understand the microstructural origin of these strength variations, the evolution of the crystalline hydration phases was investigated using in-situ XRD, providing insights into how GO interacts with the cement matrix and influences the hydration process and resultant mechanical properties.

4.3.2. Evolution of hydration phases

Fig. 11 presents the XRD patterns for both the ternary binder paste (Fig. 11a) and the GO-modified binder paste with 0.1 % GO and PCE/GO ratio of 1.25 over time (Fig. 11b). The XRD results indicate a noticeable increase in the intensity of CH peaks following the inclusion of GO in the binder paste. These findings suggest that the addition of GO nanosheets accelerates cement hydration, promoting the formation of hydration products. This trend is consistent with previous studies, which have demonstrated that the presence of GO in cement paste leads to an increase in CH peak intensity, reflecting enhanced hydration activity [19, 83,84].

Cement hydration is a complex process governed by the reactions of its primary constituents, including calcium silicates (C_3S and C_2S) and calcium aluminates. These reactions result in the formation of various hydration products, including CH, ettringite (AFt), and monosulfate (AFm) phases, which collectively contribute to the structural integrity and strength development of cementitious materials [85]. The evolution of these hydration phases directly influences the microstructural properties of the binder. The observed increase in CH peak intensity in GO-modified pastes suggests that GO serves as a catalyst in hydration reactions. GO's extensive oxygen-containing functional groups, such as hydroxyl, epoxy, and carboxyl groups, provide nucleation sites for hydration product formation. This nucleation effect facilitates the precipitation of CH crystals, thereby accelerating hydration kinetics and leading to a higher degree of hydration in the cement matrix [19]. As a result, the incorporation of GO may contribute to the early strength gain

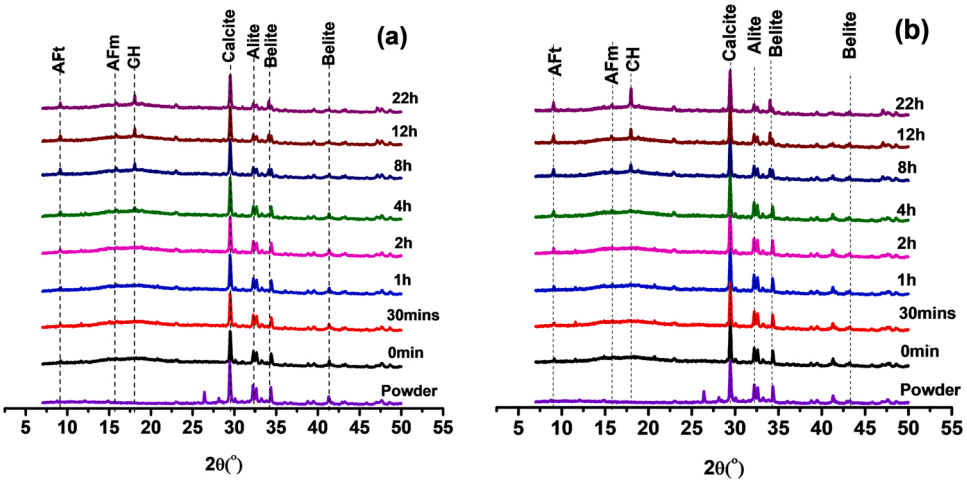

Fig. 11. In-situ XRD patterns showing the evolution of hydration phases over 22 h for (a) the control paste and (b) the paste modified with 0.1 % GO and a PCE/GO ratio of 1.25. Note: Key phases are designated as AFt (ettringite), AFm (monosulfoaluminate), and CH (calcium hydroxide).

of cement-based materials.

Concurrently with the increase in the intensity of the CH and AFt peaks, a progressive decrease in the peak intensity of the primary clinker phases, particularly alite and belite, was observed. This decrease signifies the ongoing consumption of these phases during the hydration reaction, leading to the formation of the hydrate products. This reduction suggests that the hydration of these calcium silicate phases occurs at a faster rate in the presence of GO, further reinforcing its hydration-promoting effect [86]. The increased consumption of alite and belite results in the accelerated production of C-S-H gel, the primary binding phase responsible for strength development. The present findings align with prior research demonstrating that GO promotes cement hydration and increases CH formation [19,83,84]. However, contradictory results have been reported in certain studies. Xu et al. [21] observed a decrease in CH formation in GO-modified cement pastes, which they attributed to the interaction between Ca^{2+} ions and GO. This interaction can lead to Ca^{2+} adsorption on GO nanosheets, causing agglomeration and reducing the availability of free Ca^{2+} ions required for CH precipitation [21]. This discrepancy highlights the complex role of GO in cement hydration, where its effects may vary based on factors such as dispersion quality, concentration, and interaction with cementitious ions.

The mineralogical data from XRD analysis suggest that the incorporation of GO enhances hydration reactions in the cement matrix. The increased formation of CH and C-S-H phases likely contributes to improvements in mechanical strength, as observed in the mechanical properties analysis. By promoting hydration, GO-modified pastes develop a denser microstructure, improving compressive strength and durability. This finding reinforces the potential of GO as an effective nano-additive for enhancing the performance of cementitious materials.

This direct observation of enhanced clinker consumption and accelerated formation of hydration products in the GO-modified paste provides a clear microstructural basis for the improved early-age compressive strength reported in the previous section. The increased volume of hydration products, such as CH and C-S-H, leads to a denser matrix, which is directly responsible for the observed mechanical enhancement.

4.4. *Carbonation performance of GO-modified composites*

The carbonation behaviour of the GO-modified pastes revealed a highly unexpected trend that differs from many studies on ordinary Portland cement systems. While numerous studies report that GO reduces the carbonation rate by densifying the cement matrix and refining the pore structure [44,45], our findings show a significant acceleration of the carbonation front. As presented in Fig. 12a, the sample containing 0.1 wt% GO exhibited the greatest carbonation depth at all intervals, with a calculated carbonation rate 83.7 % faster than the control. We attribute this contradictory result to the specific chemistry of the

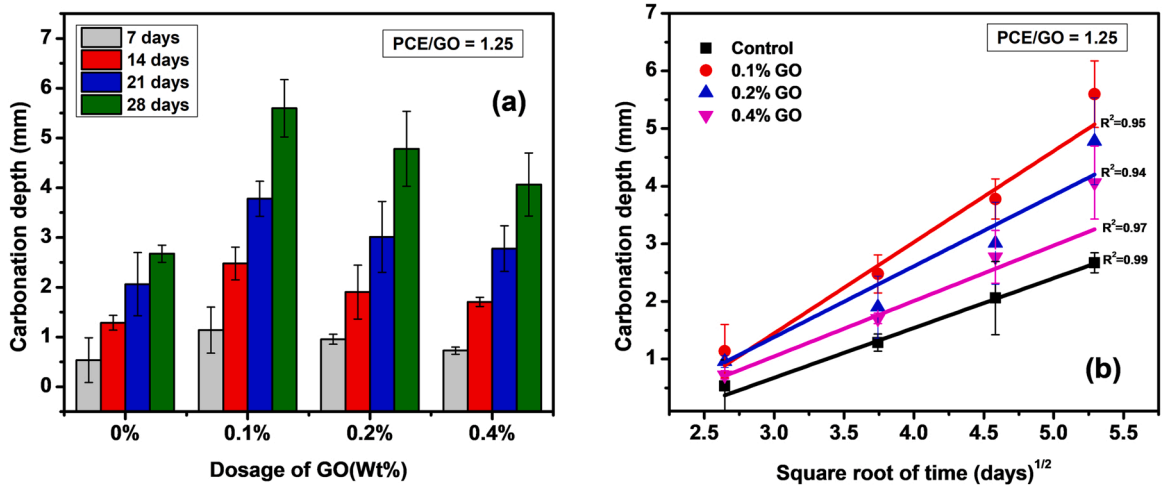

Fig. 12. Carbonation of GO-modified pastes: (a) carbonation depth over 28 days, and (b) carbonation rate derived from the square root of time.

low-clinker ternary system used. It is hypothesized that in this portlandite-limited blend, the powerful nucleation effect of GO on the precipitation of $CaCO_3$ at the surface dominates over the longer-term bulk matrix densification reported in ordinary Portland cement systems.

The progression of the carbonation front, plotted against the square root of time, is shown in Fig. 12b. The carbonation rate, determined from the slope of these lines, was 0.86 mm^2/day for control, 1.58 mm^2/day for 0.1 % GO, 1.23 mm^2/day for 0.2 % GO, and 0.96 mm^2/day for 0.4 % GO. The sample with 0.1 wt% GO had a rate of 83.7 % faster than the control. This accelerated carbonation is likely due to the well-dispersed GO nanosheets acting as nucleation sites for the precipitation of $CaCO_3$, thereby speeding up the reaction between CO_2 and the cement matrix [26–28]. The enhancement was less pronounced at higher concentrations (0.4 wt% GO), likely due to the agglomeration of GO, which reduces the available surface area for nucleation [32].

For a quantitative assessment, Fig. 13 presents the results from TGA and derivative thermogravimetry (DTG) performed on the samples after 42 days of exposure. The calculated content of CH, $CaCO_3$, and the total CO_2 uptake are summarized in Table 5. The TGA results show that the CH content is relatively similar across all samples, indicating that the carbonation process consumed the available portlandite. The calculated $CaCO_3$ content is also high in all samples, confirming a high degree of carbonation.

Furthermore, the TGA results revealed an unexpected paradox that differs from the relationships previously described in the literature. While Mishra et al. (2022) reported a "slower rate, higher uptake" relationship [28], our study identifies a "faster rate, neutral uptake" paradox. Despite having the fastest carbonation rate, the 0.1 wt% GO sample showed no corresponding increase, and in fact, a slight decrease, in total CO_2 uptake (14.62 %) compared to the control (15.22 %). This highlights a complex relationship between the kinetics of carbonation and the total sequestration capacity. A plausible explanation is a two-stage mechanism. First, the initial, rapid carbonation in the GO-modified samples is driven by the well-dispersed nanosheets acting as nucleation sites for the precipitation of $CaCO_3$, thereby accelerating the reaction [26–28]. Second, this accelerated reaction is responsible for the rapid formation of a dense, carbonated layer near the surface. Such densification is consistent with established findings that the addition of GO to cement paste leads to a significant refinement of the pore structure and a reduction in overall porosity [87]. This densification, while beneficial for mechanical properties, could then act as a barrier that inhibits the diffusion of CO_2 deeper into the sample over the long term, a mechanism that has been previously suggested to explain the role of GO in limiting long-term carbonation [46]. However, this interpretation is based on indirect evidence from carbonation depth and TGA; additional phase and microstructural characterization (e.g., XRD or SEM of carbonated samples) is required to validate the proposed mechanism.

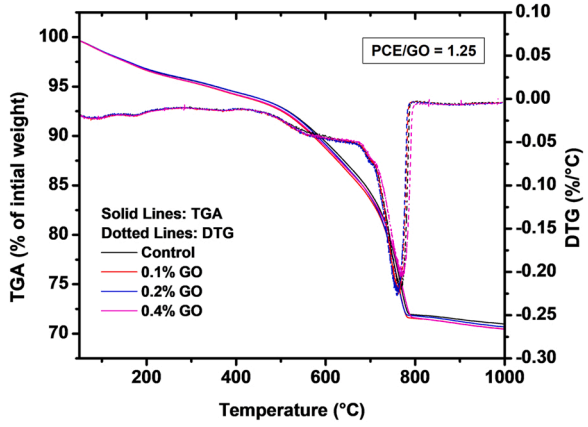

Fig. 13. TGA and DTG curves for carbonated paste samples.

Table 5
Calculated content of compounds and CO_2 uptake from TGA.

	CH (g/100 g)	$CaCO_3$ (g/100 g)	CO_2 uptake (%)
Control	6.18	45.32	15.22
0.1 % GO	6.56	45.21	14.62
0.2 % GO	6.35	45.56	15.35
0.4 % GO	6.38	45.55	14.92

This process effectively limits the volume of paste that can carbonate, thereby capping the total CO_2 uptake. This finding helps reconcile the apparent contradiction with studies such as Mishra et al. (2022) [28], which reported increased CO_2 uptake in GO-modified OPC. Standard OPC systems are rich in portlandite, offering a high potential for sequestration. In such a system, GO may promote carbonation throughout the matrix. In contrast, our low-clinker ternary blend is inherently portlandite-limited. We hypothesize that in this portlandite-limited system, the powerful kinetic effect of GO as a nucleation agent dominates, resulting in a rapid surface carbonation that forms a dense barrier. This restricts further CO_2 ingress and prevents the system from achieving a higher total uptake, thus explaining the 'faster rate, neutral uptake' paradox. Such a trade-off between early-age performance and carbonation resistance underscores the importance of tailoring mix designs to specific service conditions.

This 'faster rate, neutral uptake' paradox has significant practical implications. The accelerated early strength (as shown in Section 4.3.1) is a highly desirable outcome for applications such as precast concrete elements, as it could shorten production cycles and demolding times. However, the associated trade-off of an 83.7 % faster carbonation rate would be a major durability risk for steel-reinforced concrete structures. In such applications, the rapid progress of the carbonation front would accelerate the depassivation of the steel rebar, potentially leading to premature corrosion. This highlights the critical need to tailor GO-modified, low-clinker binders to their specific, intended application.

5. Conclusion

The impact of GO dispersion, facilitated by PCE, on the hydration kinetics, strength development, and carbonation within a low-clinker ternary blended cement system was systematically examined. The results demonstrate that PCE is essential for stabilizing GO in the alkaline cementitious environment, with a PCE/GO ratio of 10 providing optimal initial dispersion. The addition of well-dispersed GO consistently accelerated hydration, translating to significant mechanical benefits; 0.1 wt% GO yielded a 26 % increase in 1-day compressive strength, which was supported by in-situ XRD analysis showing enhanced clinker phase dissolution.

The study's primary contribution to new knowledge is the discovery of a carbonation paradox that contradicts the established literature for ordinary cements. In this low-clinker ternary system, GO was found to accelerate the carbonation rate by 83.7 %, yet this did not lead to an increase in total CO_2 sequestration. This decoupling of kinetics from ultimate capacity reveals a critical trade-off and challenges the prevailing assumption that faster carbonation equates to greater CO_2 uptake in nano-engineered binders.

This study also opens clear avenues for future research. The mechanical analysis was focused on early-age strength; future work should include 28-day data to confirm long-term performance. Furthermore, while this study's qualitative XRD data confirmed the acceleration, future quantitative Rietveld refinement is needed for a more rigorous analysis of phase evolution. Finally, the mechanisms for both the strength reduction at high GO dosages and the carbonation paradox were proposed based on performance data; a critical next step is to use direct microstructural characterization (e.g., SEM) to validate both hypotheses and to assess the scalability of these effects in larger structural elements under natural carbonation and environmental conditions.

Overall, this research demonstrates that while GO is a potent additive for enhancing the early-age performance of low-clinker cements, its practical application requires careful optimization to balance the competing and sometimes contradictory effects on hydration, strength, and long-term carbonation behavior. For practical mix design, this means engineers must co-optimize both the GO dosage and the PCE/GO ratio, recognizing that the 'optimal' GO concentration for early strength (e.g., 0.1 wt%) may differ from that required for other performance metrics.

CRediT authorship contribution statement

Suriyaprakash Saravanan: Writing – original draft, Visualization, Investigation, Formal analysis, Data curation. **Liming Huang:** Writing – review & editing, Supervision, Methodology, Conceptualization. **Arezou Babaahmadi:** Writing – review & editing, Supervision, Project administration, Methodology, Funding acquisition.

Declaration of Generative AI and AI-assisted technologies in the writing process

During the preparation of this work the author(s) used generative AI services, including Gemini (Google) and ChatGPT (OpenAI), in order to improve the language, structure, and clarity of the manuscript. After using these services, the author(s) reviewed and edited the content as needed and take full responsibility for the content of the published article.

Declaration of Competing Interest

The authors declare the following financial interests/personal relationships which may be considered as potential competing interests: Suriyaprakash Saravanan reports financial support was provided by the Swedish strategic innovation program SIO Grafen. If there are other authors, they declare that they have no known competing financial interests or personal relationships that could have appeared to influence the work reported in this paper.

Acknowledgement

The authors would like to express their gratitude to Graphenea SA for generously supplying the graphene oxide materials used in this study. Financial support for this research was provided by the Swedish Strategic Innovation Program SIO Grafen, Gothenburg, Sweden, which is gratefully acknowledged. The experimental work was performed at the Department of Architecture and Civil Engineering, Chalmers University of Technology, between 2023 and 2024, as part of the first author's master's thesis (ACEX60).

Data availability

Data will be made available on request.

References

[1] C. Chen, R. Xu, D. Tong, X. Qin, J. Cheng, J. Liu, B. Zheng, L. Yan, Q. Zhang, A striking growth of CO2 emissions from the global cement industry driven by new facilities in emerging countries, Environ. Res. Lett. 17 (2022) 044007, https://doi.org/10.1088/1748-9326/AC48B5.

[2] R.M. Andrew, Global CO2 emissions from cement production, 1928-2018, Earth Syst. Sci. Data 11 (2019) 1675–1710, https://doi.org/10.5194/ESSD-11-1675-2019.

[3] K.L. Scrivener, V.M. John, E.M. Gartner, Eco-efficient cements: potential economically viable solutions for a low-CO2 cement-based materials industry, Cem. Concr. Res. 114 (2018) 2–26, https://doi.org/10.1016/J.CEMCONRES.2018.03.015.

[4] M.C.G. Juenger, R. Siddique, Recent advances in understanding the role of supplementary cementitious materials in concrete, Cem. Concr. Res. 78 (2015) 71–80, https://doi.org/10.1016/J.CEMCONRES.2015.03.018.

[5] M. Antoni, J. Rossen, F. Martirena, K. Scrivener, Cement substitution by a combination of metakaolin and limestone, Cem. Concr. Res. 42 (2012) 1579–1589, https://doi.org/10.1016/J.CEMCONRES.2012.09.006.

[6] B. Lothenbach, K. Scrivener, R.D. Hooton, Supplementary cementitious materials, Cem. Concr. Res. 41 (2011) 1244–1256, https://doi.org/10.1016/J.CEMCONRES.2010.12.001.

[7] K. Scrivener, R. Snellings, B. Lothenbach, A practical guide to microstructural analysis of cementitious materials, A Pract. Guide Microstruct. Anal. Cem. Mater. (2016) 1–531, https://doi.org/10.1201/B19074.

[8] N. Tarannum, R. Khan, K. Pooja, Silica fume as sustainable supplementary cementitious materials in concrete, Recent Dev. Innov. Sustain. Prod. Concr. (2025) 167–183, https://doi.org/10.1016/B978-0-443-23895-6.00007-8.

[9] H.A. Dahish, M.S. Alfawzan, B.A. Tayeh, M.A. Abusogi, M. Bakri, Effect of inclusion of natural pozzolan and silica fume in cement - based mortars on the compressive strength utilizing artificial neural networks and support vector machine, Case Stud. Constr. Mater. 18 (2023) e02153, https://doi.org/10.1016/J.CSCM.2023.E02153.

[10] L. Campagiorni, M. Tonelli, F. Ridi, Synergistic effect of limestone and supplementary cementitious materials in ternary blended cements, Curr. Opin. Colloid Interface Sci. 75 (2025) 101885, https://doi.org/10.1016/J.COCIS.2024.101885.

[11] S. von Greve-Dierfeld, B. Lothenbach, A. Vollpracht, B. Wu, B. Huet, C. Andrade, C. Medina, C. Thiel, E. Gruyaert, H. Vanoutrive, I.F. Saéz del Bosque, I. Ignjatovic, J. Elsen, J.L. Provis, K. Scrivener, K.C. Thienel, K. Sideris, M. Zajac, N. Alderete, Ö. Cizer, P. Van den Heede, R.D. Hooton, S. Kamali-Bernard, S.A. Bernal, Z. Zhao, Z. Shi, N. De Belie, Understanding the carbonation of concrete with supplementary cementitious materials: a critical review by RILEM TC 281-CCC, Mater. Struct. 53 (2020), https://doi.org/10.1617/S11527-020-01558-W.

[12] V. Shah, S. Bishnoi, Carbonation resistance of cements containing supplementary cementitious materials and its relation to various parameters of concrete, Constr. Build. Mater. 178 (2018) 219–232, https://doi.org/10.1016/J.CONBUILDMAT.2018.05.162.

[13] S. Rathnarajan, B.S. Dhanya, R.G. Pillai, R. Gettu, M. Santhanam, Carbonation model for concretes with fly ash, slag, and limestone calcined clay - using accelerated and five - year natural exposure data, Cem. Concr. Compos 126 (2022), https://doi.org/10.1016/J.CEMCONCOMP.2021.104329.

[14] F. Lollini, E. Redaelli, Corrosion rate of carbon steel in carbonated concrete made with different supplementary cementitious materials, Corros. Eng. Sci. Technol. 56 (2021) 473–482, https://doi.org/10.1080/1478422X.2021.1916236.

[15] Y. Mao, X. Hu, U.J. Alengaram, W. Chen, C. Shi, Use of carbonated recycled cement paste powder as a new supplementary cementitious material: a critical review, Cem. Concr. Compos 154 (2024), https://doi.org/10.1016/J.CEMCONCOMP.2024.105783.

[16] X. Wang, J. Zhong, Revisiting the strengthening mechanisms of graphene oxide reinforced cement: effects of dispersion states, Cem. Concr. Res. 170 (2023), https://doi.org/10.1016/j.cemconres.2023.107189.

[17] T.S. Qureshi, D.K. Panesar, B. Sidhureddy, A. Chen, P.C. Wood, Nano-cement composite with graphene oxide produced from epigenetic graphite deposit, Compos. B Eng. 159 (2019) 248–258, https://doi.org/10.1016/J.COMPOSITESB.2018.09.095.

[18] W. Li, X. Li, S.J. Chen, Y.M. Liu, W.H. Duan, S.P. Shah, Effects of graphene oxide on early-age hydration and electrical resistivity of Portland cement paste, Constr. Build. Mater. 136 (2017) 506–514, https://doi.org/10.1016/J.CONBUILDMAT.2017.01.066.

[19] C. Lin, W. Wei, Y.H. Hu, Catalytic behavior of graphene oxide for cement hydration process, J. Phys. Chem. Solids 89 (2016) 128–133, https://doi.org/10.1016/J.JPCS.2015.11.002.

[20] E. Horszczaruk, E. Mijowska, R.J. Kalenczuk, M. Aleksandrzak, S. Mijowska, Nanocomposite of cement/graphene oxide – Impact on hydration kinetics and Young's modulus, Constr. Build. Mater. 78 (2015) 234–242, https://doi.org/10.1016/J.CONBUILDMAT.2014.12.009.

[21] G. Xu, S. Du, J. He, X. Shi, The role of admixed graphene oxide in a cement hydration system, Carbon N. Y 148 (2019) 141–150, https://doi.org/10.1016/J.CARBON.2019.03.072.

[22] X. Zhu, X. Kang, Effect of graphene oxide (GO) on the hydration and dissolution of alite in a synthetic cement system, J. Mater. Sci. 55 (2020) 3419–3433, https://doi.org/10.1007/S10853-019-04266-1.

[23] D. Konios, M.M. Stylianakis, E. Stratakis, E. Kymakis, Dispersion behaviour of graphene oxide and reduced graphene oxide, J. Colloid Interface Sci. 430 (2014) 108–112, https://doi.org/10.1016/J.JCIS.2014.05.033.

[24] X. Kang, X. Zhu, J. Liu, X. Shu, J. Qian, Y. Huang, Hydration of C3A/gypsum composites in the presence of graphene oxide, Mater. Today Commun. 23 (2020) 100889, https://doi.org/10.1016/J.MTCOMM.2019.100889.

[25] A. Gladwin Alex, A. Kedir, T. Gebrehiwet Tewele, Review on effects of graphene oxide on mechanical and microstructure of cement-based materials, Constr. Build. Mater. 360 (2022), https://doi.org/10.1016/J.CONBUILDMAT.2022.129609.

[26] D. Zheng, H. Yang, F. Yu, B. Zhang, H. Cui, Effect of graphene oxide on the crystallization of calcium carbonate by C3S carbonation, Materials 12 (2019), https://doi.org/10.3390/MA12132045.

[27] S.A. Yaseen, G.A. Yiseen, Z. Li, Elucidation of calcite structure of calcium carbonate formation based on hydrated cement mixed with graphene oxide and reduced graphene oxide, ACS Omega 4 (2019) 10160–10170, https://doi.org/10.1021/ACSOMEGA.9B00042.

[28] G. Mishra, A. Warda, S.P. Shah, Carbon sequestration in graphene oxide modified cementitious system, J. Build. Eng. 62 (2022) 105356, https://doi.org/10.1016/J.JOBE.2022.105356.

[29] S. Stankovich, D.A. Dikin, R.D. Piner, K.A. Kohlhaas, A. Kleinhammes, Y. Jia, Y. Wu, S.B.T. Nguyen, Synthesis of graphene-based nanosheets via chemical reduction of exfoliated graphite oxide, Carbon 45 (2007) 1558–1565, https://doi.org/10.1016/j.carbon.2007.02.034.
[30] L. Zhao, S. Zhu, H. Wu, X. Zhang, Q. Tao, L. Song, Y. Song, X. Guo, Deep research about the mechanisms of graphene oxide (GO) aggregation in alkaline cement pore solution, Constr. Build. Mater. 247 (2020), https://doi.org/10.1016/J.CONBUILDMAT.2020.118446.
[31] S. Ghazizadeh, P. Duffour, N.T. Skipper, M. Billing, Y. Bai, An investigation into the colloidal stability of graphene oxide nano-layers in alite paste, Cem. Concr. Res. 99 (2017) 116–128, https://doi.org/10.1016/j.cemconres.2017.05.011.
[32] X. Li, Y.M. Liu, W.G. Li, C.Y. Li, J.G. Sanjayan, W.H. Duan, Z. Li, Effects of graphene oxide agglomerates on workability, hydration, microstructure and compressive strength of cement paste, Constr. Build. Mater. 145 (2017) 402–410, https://doi.org/10.1016/J.CONBUILDMAT.2017.04.058.
[33] Z. Lu, D. Hou, A. Hanif, W. Hao, G. Sun, Z. Li, Comparative evaluation on the dispersion and stability of graphene oxide in water and cement pore solution by incorporating silica fume, Cem. Concr. Compos 94 (2018) 33–42, https://doi.org/10.1016/J.CEMCONCOMP.2018.08.011.
[34] C. Stephens, L. Brown, F. Sanchez, Quantification of the re-agglomeration of carbon nanofiber aqueous dispersion in cement pastes and effect on the early age flexural response, Carbon N. Y 107 (2016) 482–500, https://doi.org/10.1016/J.CARBON.2016.05.076.
[35] M.S. Strano, V.C. Moore, M.K. Miller, M.J. Allen, E.H. Haroz, C. Kittrell, R. H. Hauge, R.E. Smalley, The role of surfactant adsorption during ultrasonication in the dispersion of single-walled carbon nanotubes, J. Nanosci. Nanotechnol. 3 (2003) 81–86, https://doi.org/10.1166/JNN.2003.194.
[36] Z. Lu, D. Hou, L. Meng, G. Sun, C. Lu, Z. Li, Mechanism of cement paste reinforced by graphene oxide/carbon nanotubes composites with enhanced mechanical properties, RSC Adv. 5 (2015) 100598–100605, https://doi.org/10.1039/C5RA18602A.
[37] S. Parveen, S. Rana, R. Fangueiro, M.C. Paiva, Microstructure and mechanical properties of carbon nanotube reinforced cementitious composites developed using a novel dispersion technique, Cem. Concr. Res. 73 (2015) 215–227, https://doi.org/10.1016/J.CEMCONRES.2015.03.006.
[38] Q. Li, C. He, H. Zhou, Z. Xie, D. Li, Effects of polycarboxylate superplasticizer-modified graphene oxide on hydration characteristics and mechanical behavior of cement, Constr. Build. Mater. 272 (2021), https://doi.org/10.1016/J.CONBUILDMAT.2020.121904.
[39] H. Zhang, X. Gan, Z. Lu, L. Li, L. Lu, Polycarboxylate superplasticizer-modified graphene oxide: dispersion and performance enhancement in cement paste, Nanomaterials 15 (2025), https://doi.org/10.3390/NANO15060419.
[40] B. Liu, L. Wang, G. Pan, D. Li, Dispersion of graphene oxide modified polycarboxylate superplasticizer in cement alkali solution for improving cement composites, J. Build. Eng. 57 (2022), https://doi.org/10.1016/J.JOBE.2022.104860.
[41] L. Zhao, X. Guo, Y. Liu, C. Ge, Z. Chen, L. Guo, X. Shu, J. Liu, Investigation of dispersion behavior of GO modified by different water reducing agents in cement pore solution, Carbon N. Y 127 (2018) 255–269, https://doi.org/10.1016/J.CARBON.2017.11.016.
[42] J. Li, Q. Zheng, The first experimental evidence for improved nanomechanical properties of calcium silicate hydrate by polycarboxylate ether and graphene oxide, Cem. Concr. Res. 156 (2022), https://doi.org/10.1016/j.cemconres.2022.106787.
[43] S. Ghazizadeh, P. Duffour, N.T. Skipper, Y. Bai, Understanding the behaviour of graphene oxide in Portland cement paste, Cem. Concr. Res. 111 (2018) 169–182, https://doi.org/10.1016/J.CEMCONRES.2018.05.016.
[44] A. Mohammed, J.G. Sanjayan, A. Nazari, A. Bagheri, N.T.K. Al-Saadi, Inhibition of carbonation attack in cement-based matrix due to adding graphene oxide, Aust. J. Civ. Eng. 15 (2017) 20–31, https://doi.org/10.1080/14488353.2017.1367252.
[45] J. Gong, Y. Qian, Z. Xu, C. Chen, Y. Jin, J. Zhang, Z. Li, X. Shi, Effect of graphene oxide on the properties of ternary limestone clay cement paste, Nanotechnol. Rev. 13 (2024), https://doi.org/10.1515/NTREV-2023-0222.
[46] A. Mohammed, J.G. Sanjayan, A. Nazari, N.T.K. Al-Saadi, The role of graphene oxide in limited long-term carbonation of cement-based matrix, Constr. Build. Mater. 168 (2018) 858–866, https://doi.org/10.1016/J.CONBUILDMAT.2018.02.082.
[47] W.J. McCarter, T.M. Chrisp, G. Starrs, A. Adamson, P.A.M. Basheer, S. V. Nanukuttan, S. Srinivasan, C. Green, Characterization of physio-chemical processes and hydration kinetics in concretes containing supplementary cementitious materials using electrical property measurements, Cem. Concr. Res. 50 (2013) 26–33, https://doi.org/10.1016/J.CEMCONRES.2013.03.008.
[48] L. Huang, Water and alkali salts in the hydrating and hardened green cement-based materials: Hydration process, moisture content and transport, 2022, ⟨https://research.chalmers.se/en/publication/528441⟩.
[49] L. Huang, L. Tang, I. Löfgren, N. Olsson, Z. Yang, Real-time monitoring the electrical properties of pastes to map the hydration induced microstructure change in cement-based materials, Cem. Concr. Compos 132 (2022) 104639, https://doi.org/10.1016/J.CEMCONCOMP.2022.104639.
[50] H. Mehdizadeh, X. Jia, K.H. Mo, T.C. Ling, Effect of water-to-cement ratio induced hydration on the accelerated carbonation of cement pastes, Environ. Pollut. 280 (2021) 116914, https://doi.org/10.1016/J.ENVPOL.2021.116914.
[51] K. Amini, S. Soleimani Amiri, A. Ghasemi, S. Mirvalad, A. Habibnejad Korayem, Evaluation of the dispersion of metakaolin–graphene oxide hybrid in water and cement pore solution: can metakaolin really improve the dispersion of graphene oxide in the calcium-rich environment of hydrating cement matrix? RSC Adv. 11 (2021) 18623–18636, https://doi.org/10.1039/D1RA01504D.
[52] W. Qin, Q. Guodong, Z. Dafu, W. Yue, Z. Haiyu, Influence of the molecular structure of a polycarboxylate superplasticiser on the dispersion of graphene oxide in cement pore solutions and cement-based composites, Constr. Build. Mater. 272 (2021), https://doi.org/10.1016/J.CONBUILDMAT.2020.121969.
[53] J. Plank, F. Yang, O. Storcheva, Study of the interaction between cement phases and polycarboxylate superplasticizers possessing silyl functionalities, J. Sustain. Cem. Based Mater. 3 (2014) 77–87, https://doi.org/10.1080/21650373.2014.903382.
[54] Y. Zhou, Q. Bao, L.A.L. Tang, Y. Zhong, K.P. Loh, Hydrothermal dehydration for the "green" reduction of exfoliated graphene oxide to graphene and demonstration of tunable optical limiting properties, Chem. Mater. 21 (2009) 2950–2956, https://doi.org/10.1021/CM9006603.
[55] E.K. Walker, D.A. Vanden Bout, K.J. Stevenson, Spectroelectrochemical investigation of an electrogenerated graphitic oxide solid-electrolyte interphase, Anal. Chem. 84 (19) (2012) 8190–8197, https://doi.org/10.1021/AC3014252.
[56] X. Fan, W. Peng, Y. Li, X. Li, S. Wang, G. Zhang, F. Zhang, Deoxygenation of exfoliated graphite oxide under alkaline conditions: a green route to graphene preparation, Adv. Mater. 20 (2008) 4490–4493, https://doi.org/10.1002/ADMA.200801306.
[57] J.S. Lauret, C. Voisin, G. Cassabois, C. Delalande, P. Roussignol, O. Jost, L. Capes, Ultrafast carrier dynamics in single-wall carbon nanotubes, Phys. Rev. Lett. 90 (2003) 057404, https://doi.org/10.1103/PHYSREVLETT.90.057404.
[58] Q. Lai, S. Zhu, X. Luo, M. Zou, S. Huang, Ultraviolet-visible spectroscopy of graphene oxides, AIP Adv. 2 (2012) 32146, https://doi.org/10.1063/1.4747817.
[59] W. Mäntele, E. Deniz, UV–VIS absorption spectroscopy: Lambert-Beer reloaded, Spectrochim. Acta A Mol. Biomol. Spectrosc. 173 (2017) 965–968, https://doi.org/10.1016/J.SAA.2016.09.037.
[60] A.J. Blanch, C.E. Lenehan, J.S. Quinton, Optimizing surfactant concentrations for dispersion of single-walled carbon nanotubes in aqueous solution, J. Phys. Chem. B 114 (2010) 9805–9811, https://doi.org/10.1021/JP104113D.
[61] R. Kaur, K. Bhatrola, A. Kumar, J. Kaur, S. Suhag, S.K. Maurya, N.C. Kothiyal, Durability of cementitious mortar: incorporation of highly dispersed superplasticizer modified graphene oxide in fly ash blended mortar, J. Build. Eng. 80 (2023), https://doi.org/10.1016/J.JOBE.2023.107888.
[62] A. Zingg, F. Winnefeld, L. Holzer, J. Pakusch, S. Becker, R. Figi, L. Gauckler, Interaction of polycarboxylate-based superplasticizers with cements containing different C3A amounts, Cem. Concr. Compos 31 (2009) 153–162, https://doi.org/10.1016/J.CEMCONCOMP.2009.01.005.
[63] S. Liu, T.H. Zeng, M. Hofmann, E. Burcombe, J. Wei, R. Jiang, J. Kong, Y. Chen, Antibacterial activity of graphite, graphite oxide, graphene oxide, and reduced graphene oxide: membrane and oxidative stress, ACS Nano 5 (2011) 6971–6980, https://doi.org/10.1021/NN202451X.
[64] M. Lotya, A. Rakovich, J.F. Donegan, J.N. Coleman, Measuring the lateral size of liquid-exfoliated nanosheets with dynamic light scattering, Nanotechnology 24 (2013) 265703, https://doi.org/10.1088/0957-4484/24/26/265703.
[65] M. Wang, X. Ji, H. Manzano, D. Hou, Z. Li, Unlocking cementitious performance: nano-lubrication via polycarboxylate superplasticizers, J. Am. Ceram. Soc. 107 (2024) 3055–3067, https://doi.org/10.1111/JACE.19643.
[66] S. Park, K.S. Lee, G. Bozoklu, W. Cai, S.B.T. Nguyen, R.S. Ruoff, Graphene oxide papers modified by divalent ions - Enhancing mechanical properties via chemical cross-linking, ACS Nano 2 (2008) 572–578, https://doi.org/10.1021/NN700349A.
[67] L. Wu, L. Liu, B. Gao, R. Muñoz-Carpena, M. Zhang, H. Chen, Z. Zhou, H. Wang, Aggregation kinetics of graphene oxides in aqueous solutions: experiments, mechanisms, and modeling, Langmuir 29 (2013) 15174–15181, https://doi.org/10.1021/LA404134X.
[68] J. Stecher, J. Plank, Adsorbed layer thickness of polycarboxylate and polyphosphate superplasticizers on polystyrene nanoparticles measured via dynamic light scattering, J. Colloid Interface Sci. 562 (2020) 204–212, https://doi.org/10.1016/J.JCIS.2019.11.108.
[69] H. Chi, C. Wang, Y. Tian, Z. Xie, Q. Yuan, Z. Chen, X. Zhu, Unraveling polycarboxylate superplasticizer (PCE) compatibility in muscovite-blended cement paste through aggregation mechanisms, J. Build. Eng. 95 (2024), https://doi.org/10.1016/J.JOBE.2024.110133.
[70] Y. Zhang, X. Kong, Correlations of the dispersing capability of NSF and PCE types of superplasticizer and their impacts on cement hydration with the adsorption in fresh cement pastes, Cem. Concr. Res. 69 (2015) 1–9, https://doi.org/10.1016/J.CEMCONRES.2014.11.009.
[71] Z. Pan, L. He, L. Qiu, A.H. Korayem, G. Li, J.W. Zhu, F. Collins, D. Li, W.H. Duan, M.C. Wang, Mechanical properties and microstructure of a graphene oxide–cement composite, Cem. Concr. Compos 58 (2015) 140–147, https://doi.org/10.1016/J.CEMCONCOMP.2015.02.001.
[72] A. Mohammed, J.G. Sanjayan, W.H. Duan, A. Nazari, Incorporating graphene oxide in cement composites: a study of transport properties, Constr. Build. Mater. 84 (2015) 341–347, https://doi.org/10.1016/J.CONBUILDMAT.2015.01.083.
[73] Q. Wang, J. Wang, C.X. Lu, B.W. Liu, K. Zhang, C.Z. Li, Influence of graphene oxide additions on the microstructure and mechanical strength of cement, N. Carbon Mater. 30 (2015) 349–356, https://doi.org/10.1016/S1872-5805(15)60194-9.
[74] F. Ridi, L. Dei, E. Fratini, S.H. Chen, P. Baglioni, Hydration kinetics of tri-calcium silicate in the presence of superplasticizers, J. Phys. Chem. B 107 (2003) 1056–1061, https://doi.org/10.1021/JP027346B.
[75] C. Legrand, E. Wirquin, Study of the strength of very young concrete as a function of the amount of hydrates formed-influence of superplasticizer, Mater. Struct. 27 (1994) 106–109, https://doi.org/10.1007/BF02472828.

[76] S. Meng, X. Ouyang, J. Fu, Y. Niu, Y. Ma, The role of graphene/graphene oxide in cement hydration, Nanotechnol. Rev. 10 (2021) 768–778, https://doi.org/10.1515/NTREV-2021-0055.
[77] K. Gong, Z. Pan, A.H. Korayem, L. Qiu, D. Li, F. Collins, C.M. Wang, W.H. Duan, Reinforcing effects of graphene oxide on portland cement paste, J. Mater. Civ. Eng. 27 (2015) A4014010, https://doi.org/10.1061/(ASCE)MT.1943-5533.0001125.
[78] F. Babak, H. Abolfazl, R. Alimorad, G. Parviz, Preparation and mechanical properties of graphene oxide: cement nanocomposites, Sci. World J. 2014 (2014) 276323, https://doi.org/10.1155/2014/276323.
[79] W. Stumm, L. Sigg, B. Sulzberger, Chemistry of the solid-water interface: processes at the mineral-water and particle-water interface in natural systems, (1992) 428. ⟨https://www.wiley.com/en-us/Chemistry+of+the+Solid-Water+Interface%3A+Processes+at+the+Mineral-Water+and+Particle-Water+Interface+in+<underline>Natural</underline>+Systems-p-9780471576723⟩.
[80] A. Mohammed, J.G. Sanjayan, W.H. Duan, A. Nazari, Graphene oxide impact on hardened cement expressed in enhanced freeze–thaw resistance, J. Mater. Civ. Eng. 28 (2016) 04016072, https://doi.org/10.1061/(ASCE)MT.1943-5533.0001586.
[81] M. Saafi, L. Tang, J. Fung, M. Rahman, J. Liggat, Enhanced properties of graphene/fly ash geopolymeric composite cement, Cem. Concr. Res. 67 (2015) 292–299, https://doi.org/10.1016/J.CEMCONRES.2014.08.011.
[82] I.G. Richardson, A.V. Girão, R. Taylor, S. Jia, Hydration of water- and alkali-activated white Portland-based cement pastes and blends with low-calcium pulverized fuel ash, Cem. Concr. Res. 83 (2016) 1–18, https://doi.org/10.1016/J.CEMCONRES.2016.01.008.
[83] S. Lv, S. Ting, J. Liu, Q. Zhou, Use of graphene oxide nanosheets to regulate the microstructure of hardened cement paste to increase its strength and toughness, CrystEngComm 16 (2014) 8508–8516, https://doi.org/10.1039/C4CE00684D.
[84] L. Wang, S. Zhang, D. Zheng, H. Yang, H. Cui, W. Tang, D. Li, Effect of Graphene Oxide (GO) on the morphology and microstructure of cement hydration products, Nanomaterials 7 (2017) 429, https://doi.org/10.3390/NANO7120429.
[85] S. Chakraborty, S.P. Kundu, A. Roy, B. Adhikari, S.B. Majumder, Effect of jute as fiber reinforcement controlling the hydration characteristics of cement matrix, Ind. Eng. Chem. Res. 52 (2013) 1252–1260, https://doi.org/10.1021/IE300607R.
[86] X. Kang, X. Zhu, J. Liu, X. Shu, Y. Huang, J. Qian, Dissolution and precipitation behaviours of graphene oxide / tricalcium silicate composites, Compos. Part BEng. 186 (2020) 107800, https://doi.org/10.1016/J.COMPOSITESB.2020.107800.
[87] C. Ruan, J. Lin, S. Chen, K. Sagoe-Crentsil, W. Duan, Effect of graphene oxide on the pore structure of cement paste: implications for performance enhancement, ACS Appl. Nano Mater. 4 (2021) 10623–10633, https://doi.org/10.1021/ACSANM.1C02090.